APPROVED FOR PUBLIC RELEASE, DISTRIBUTION UNLIMITED

ALEX(01)-TR-77-04

LEVEL II

AUTOMATIC DETECTION, TIMING AND PRELIMINARY DISCRIMINATION OF SEISMIC SIGNALS WITH THE INSTANTANEOUS AMPLITUDE, PHASE AND FREQUENCY

12

TECHNICAL REPORT NO. 4
VELA NETWORK EVALUATION AND AUTOMATIC PROCESSING RESEARCH

Prepared by
Rudolf Unger

TEXAS INSTRUMENTS INCORPORATED
Equipment Group
Post Office Box 6015
Dallas, Texas 75222

Prepared for

AIR FORCE TECHNICAL APPLICATIONS CENTER
Alexandria, Virginia 22314

Sponsored by

ADVANCED RESEARCH PROJECTS AGENCY
Nuclear Monitoring Research Office
ARPA Program Code No. 7F10
ARPA Order No. 2551

27 March 1978

Acknowledgment: This research was supported by the Advanced Research Projects Agency, Nuclear Monitoring Research Office, under Project VELA-UNIFORM, and accomplished under the technical direction of the Air Force Technical Applications Center under Contract Number F08606-77-C-0004.

APPROVED FOR PUBLIC RELEASE, DISTRIBUTION UNLIMITED

(14) TI-ALEX(01)-TR-77-04

(6) # AUTOMATIC DETECTION, TIMING AND PRELIMINARY DISCRIMINATION OF SEISMIC SIGNALS WITH THE INSTANTANEOUS AMPLITUDE, PHASE AND FREQUENCY

(9) TECHNICAL REPORT NO. 4
VELA NETWORK EVALUATION AND AUTOMATIC PROCESSING RESEARCH

Prepared by
(10) Rudolf Unger

(12) 83 p.

TEXAS INSTRUMENTS INCORPORATED
Equipment Group
Post Office Box 6015
Dallas, Texas 75222

Prepared for

AIR FORCE TECHNICAL APPLICATIONS CENTER
Alexandria, Virginia 22314

Sponsored by

ADVANCED RESEARCH PROJECTS AGENCY
Nuclear Monitoring Research Office
ARPA Program Code No. 7F10
ARPA Order No. 2551

(11) 27 March 1978

Acknowledgment: This research was supported by the Advanced Research Projects Agency, Nuclear Monitoring Research Office, under Project VELA-UNIFORM, and accomplished under the technical direction of the Air Force Technical Applications Center under Contract Number (15) F08606-77-C-0004, ARPA Order-2551

UNCLASSIFIED

SECURITY CLASSIFICATION OF THIS PAGE *(When Data Entered)*

REPORT DOCUMENTATION PAGE		READ INSTRUCTIONS BEFORE COMPLETING FORM
1. REPORT NUMBER	2. GOVT ACCESSION NO.	3. RECIPIENT'S CATALOG NUMBER
4. TITLE *(and Subtitle)* AUTOMATIC DETECTION, TIMING AND PRELIMINARY DISCRIMINATION OF SEISMIC SIGNALS WITH THE INSTANTANEOUS AMPLITUDE, PHASE AND FREQUENCY		5. TYPE OF REPORT & PERIOD COVERED: Technical 6. PERFORMING ORG. REPORT NUMBER: ALEX(01)-TR-77-04
7. AUTHOR(s): Rudolf Unger		8. CONTRACT OR GRANT NUMBER(s): F08606-77-C-0004
9. PERFORMING ORGANIZATION NAME AND ADDRESS: Texas Instruments Incorporated, Equipment Group, Dallas, Texas 75222		10. PROGRAM ELEMENT, PROJECT, TASK AREA & WORK UNIT NUMBERS: VELA T/7705/B/ETR
11. CONTROLLING OFFICE NAME AND ADDRESS: Advanced Research Projects Agency, Nuclear Monitoring Research Office, Arlington, Virginia 22209		12. REPORT DATE: 27 March 1978 13. NUMBER OF PAGES: 81
14. MONITORING AGENCY NAME & ADDRESS *(if different from Controlling Office)*: Air Force Technical Applications Center, VELA Seismological Center, Alexandria, Virginia 22314		15. SECURITY CLASS. *(of this report)*: UNCLASSIFIED 15a. DECLASSIFICATION/DOWNGRADING SCHEDULE

16. DISTRIBUTION STATEMENT *(of this Report)*

APPROVED FOR PUBLIC RELEASE, DISTRIBUTION UNLIMITED

17. DISTRIBUTION STATEMENT *(of the abstract entered in Block 20, if different from Report)*

18. SUPPLEMENTARY NOTES

ARPA Order No. 2551

19. KEY WORDS *(Continue on reverse side if necessary and identify by block number)*

Signal detection	Instantaneous phase
Signal timing	Instantaneous frequency
Seismic event discrimination	Complex envelope
Instantaneous amplitude	Envelope

20. ABSTRACT *(Continue on reverse side if necessary and identify by block number)*

The feasibility is evaluated of applying instantaneous amplitude, phase and frequency measurements to automatically detect, time and identify seismic events. Detection based on phase measurements is shown to be in principle 6 dB more sensitive than detection based on amplitude measurements. A phase detection and timing algorithm, using a priori known dispersion characteristics, is demonstrated to time the onset of simulated

DD FORM 1 JAN 73 1473 EDITION OF 1 NOV 65 IS OBSOLETE

UNCLASSIFIED

SECURITY CLASSIFICATION OF THIS PAGE *(When Data Entered)*

78 17 08 113

20. continued

teleseismic long-period surface waves within 30 seconds accuracy in 70% of the tested cases, for waveforms down to 0 dB signal-to-noise ratio. By phase measurement, rather than by amplitude measurement, this algorithm also provides a measure of the surface wave signal-to-noise ratio. These results can be applied in the extraction of weak surface waves.

Phase detection of teleseismic short-period bodywaves was not found to be feasible, due to the interference of early-arriving secondary signals. Therefore, short-period P-wave detection and timing are performed essentially by envelope peak detection; instantaneous frequency measurements are also used in the timing process. Tested on a small data base, this method resulted in 81% to 94% detection at 7 to 20 false alarms per hour, with signal-to-noise ratio thresholds of 2 to 3 dB. The RMS timing error, relative to analyst picks, was 0.21 seconds, comprising 84% of the test cases; this timing error apparently was independent of the signal-to-noise ratio. In some cases, however, noise can obscure the true signal onset for the analyst as well as for the automatic timing algorithm. Emergent signals may cause timing errors of several seconds. Measurements of the instantaneous frequency permit analysis of the delay times of secondary signals partially overlapping with earlier primary signals, down to the primary signal detection level.

Simultaneous measurements of the mean instantaneous frequency and the amount of instantaneous phase fluctuation over the first few seconds after the short-period primary signal onset provided significant separation between the populations of shallow Eurasian earthquakes, Russian presumed nuclear explosions (including peaceful explosions), and Nevada Test Site presumed nuclear explosions, even at signal-to-noise ratios below 0 dB.

ABSTRACT

The feasibility is evaluated of applying instantaneous amplitude, phase and frequency measurements to automatically detect, time and identify seismic events. Detection based on phase measurements is shown to be in principle 6 dB more sensitive than detection based on amplitude measurements. A phase detection and timing algorithm, using a priori known dispersion characteristics, is demonstrated to time the onset of simulated teleseismic long-period surface waves within 30 seconds accuracy in 70% of the tested cases, for waveforms down to 0 dB signal-to-noise ratio. By phase measurement, rather than by amplitude measurement, this algorithm also provides a measure of the surface wave signal-to-noise ratio. These results can be applied in the extraction of weak surface waves.

Phase detection of teleseismic short-period bodywaves was not found to be feasible, due to the interference of early-arriving secondary signals. Therefore, short-period P-wave detection and timing are performed essentially by envelope peak detection; instantaneous frequency measurements are also used in the timing process. Tested on a small data base, this method resulted in 81% to 94% detection at 7 to 20 false alarms per hour, with signal-to-noise ratio thresholds of 2 to 3 dB. The RMS timing error, relative to analyst picks, was 0.21 seconds, comprising 84% of the test cases; this timing error apparently was independent of the signal-to-noise ratio. In some cases, however, noise can obscure the true signal onset for the analyst as well as for the automatic timing algorithm. Emergent signals may cause timing errors of several seconds. Measurements of the instantaneous frequency permit analysis of the delay times of secondary signals partially overlapping with earlier primary signals, down to the primary signal detection level.

Simultaneous measurements of the mean instantaneous frequency and the amount of instantaneous phase fluctuation over the first few seconds after the short-period primary signal onset provided significant separation between the populations of shallow Eurasian earthquakes, Russian presumed nuclear explosions (including peaceful explosions), and Nevada Test Site presumed nuclear explosions, even at signal-to-noise ratios below 0 dB.

ACKNOWLEDGMENTS

Discussions with and suggestions by Dr. R. L. Sax, program manager, contributed strongly to this study. The figures and the text were prepared for printing by Mrs. C. B. Saunders and Mrs. K. Vitale.

TABLE OF CONTENTS

TABLE OF CONTENTS
(continued)

LIST OF FIGURES

LIST OF FIGURES
(continued)

LIST OF TABLES

SECTION I
INTRODUCTION

The use of the instantaneous amplitude, phase, and frequency is well known in communications technology (e.g., Schwartz et al., 1966; Papoulis, 1965), but has not found wide acceptance in the analysis of signals from seismic events. Potential seismic applications of the above parameters have been suggested by Farnbach (1975) and Unger (1976a, 1976b, 1976c).

In the concept of a world-wide seismic surveillance system (Sax et al., 1974; Sax, 1976) automatic detection and accurate timing of seismic signals at the station level is important, first, for hypocenter determination of associated signals detected at different stations; second, for retrieving waveforms of the located events. For the latter purpose, it is helpful, in determining the amount of data to retrieve, to have some preliminary indication if the signal stems from a nuclear explosion or from an earthquake. A special application of long-period signal timing is for time-variant, dispersion-related filtering (Unger, 1976b), aimed at estimating weak surface waves. For that application, the onset of a dispersed wave group must be determined within approximately 50 seconds accuracy.

The purpose of this study is to develop, and subsequently evaluate, algorithms for the automatic detection and timing of seismic signals, both short-period and long-period, using the instantaneous amplitude, phase, and frequency. Since some of the above mentioned potential applications concern discrimination between earthquakes and nuclear explosions, this potential was also examined briefly.

The organization of this report is as follows. Section II presents the theory for statistical amplitude and phase detection. Based on this theory, the short-period and long-period detection and timing algorithms are developed in Section III. Section IV describes and discusses the evaluation of these algorithms on a limited data base. In Section V the discrimination potential of the instantaneous amplitude, phase, and frequency is investigated. Finally, Section VI summarizes the study. A central part of the detection, timing and discrimination algorithm, the moving-window phase regression, and other details are treated in the appendices.

SECTION II
THEORY

A. INTRODUCTION

This work studies the use of the instantaneous amplitude, phase and frequency in the detection and timing of primary and secondary short-period (SP) and long-period (LP) signals. In this section, we first define the above parameters, and present the method of their computation. Next, vector diagram geometry leads us to a definition of the algorithm's SP and LP signal detection criteria.

B. *THE INSTANTANEOUS AMPLITUDE, PHASE AND FREQUENCY*

Any waveform r(t) can be expressed in terms of its instantaneous amplitude and its instantaneous frequency, or, equivalently, its instantaneous amplitude and its instantaneous phase with respect to a given monochromatic waveform:

$$r(t) = R(t) \cos\left[2\pi \int f(t)dt\right] \qquad \text{(II-1)}$$

or

$$r(t) = R(t) \cos\left[2\pi f_o t + \phi(t)\right] , \qquad \text{(II-2)}$$

where

$R(t)$ is the instantaneous amplitude (also called the "envelope"),

$f(t)$ is the instantaneous frequency,

f_o is an arbitrary reference frequency,

$\phi(t)$ is the instantaneous phase with respect to a monochromatic waveform of frequency f_o Hz and zero phase.

Thus, either R(t) and f(t), or the combination of R(t), f_o and $\phi(t)$ completely define and describe a given waveform r(t). R(t) and the angular argument of the cosine function may be viewed as the modulus and the argument, respectively, of a waveform vector or phasor r(t), or as its polar coordinates. They also reflect the amplitude modulation and the frequency or phase modulation of the waveform. Farnbach (1975) called the combination of modulus and argument the "complex envelope". The use of the above parameters and complex waveforms is found frequently in communications technology literature. Complex waveforms are not a necessity in our treatment, however. The parameter definition is illustrated in Figure II-1.

The reference frequency may be chosen arbitrarily. Since the total angular argument represents the instantaneous phase with respect to direct current (d.c., f_o=0 Hz), much of its linear contribution can be eliminated by choosing f_o as the center frequency of the waveform's dominant frequency band. This increases the display resolution of the instantaneous phase function. The monochromatic waveform of frequency f_o Hz here plays the role of the "carrier" wave as used in communication techniques.

Contrary to frequently encountered concepts stemming from analogue communication techniques, the above expressions are not subject to waveform bandwidth restrictions other than that the frequency "modulation" be no deeper than f_o Hz, in order not to exceed d.c. into the negative frequencies. In fact, the detection of secondary signals by amplitude or phase discontinuity determination, requires the waveform's entire bandwidth.

The instantaneous amplitude, phase and frequency can be obtained with the Hilbert transform, defined as

$$\overset{\vee}{r}(t) = \pi^{-1} \int_{-\infty}^{\infty} \frac{r(\tau)}{t - \tau} \, d\tau \quad . \qquad \text{(II-3)}$$

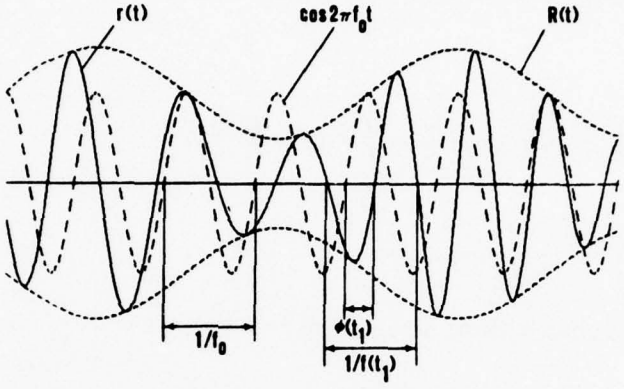

$$r(t) = R(t) \cos \left[2\pi \int f(t)\, dt \right]$$

Or:

$$r(t) = R(t) \cos \left[2\pi f_0 t + \phi(t) \right]$$

FIGURE II-1

WAVEFORM REPRESENTATION

This is the convolution of the original waveform with the function $(\pi t)^{-1}$, also known as a quadrature filter (Papoulis, 1965), or a 90^{o} phase-shift operator (Schwartz et al., 1966). The latter means transforming the original waveform representation of Equations (II-1) and (II-2) into:

$$\overset{\vee}{r}(t) = R(t) \sin \left[2\pi \int f(t)\, dt\right] \tag{II-4}$$

and

$$\overset{\vee}{r}(t) = R(t) \sin \left[2\pi f_o t + \phi(t)\right] . \tag{II-5}$$

The amplitude and phase then are resolved by:

$$R(t) = \left[r^2(t) + \overset{\vee}{r}^2(t)\right]^{\frac{1}{2}} \tag{II-6}$$

and

$$\phi(t) = \arctan \frac{\overset{\vee}{r}(t)}{r(t)} \pm k \cdot 2\pi - 2\pi f_o t , \tag{II-7}$$

where $k = 0, 1, 2,$ etc.

The $\pm k \cdot 2\pi$ ambiguity may pose a problem for high frequency waveforms, because of the high rate of change of the arctangent argument. To reduce this ambiguity, we bring the term $-2\pi f_o t$ inside the arctangent argument through trigonometric relations:

$$\phi(t) = \arctan\left[\frac{-r(t) \sin 2\pi f_o t + \overset{\vee}{r}(t) \cos 2\pi f_o t}{r(t) \cos 2\pi f_o t + \overset{\vee}{r}(t) \sin 2\pi f_o t}\right] \pm k \cdot 2\pi . \tag{II-8}$$

The maximum rate of change of phase with respect to time is now determined by the difference between the bandlimit frequencies and f_o. The NORSAR SP data, used in the SP evaluation in this study, has been anti-alias filtered at 5 Hz for a 10-Hz sampling rate. Thus, for a worst case situation in which

we (unlikely) would choose $f_o = 0$ Hz or $f_o = 5$ Hz in a 0-5 Hz bandwidth waveform, the maximum rate of phase change is 0.5 cycle per sample. The same holds true for LP waveforms which usually are bandpassed so that the waveform energy above 0.06 Hz is negligible, and sampled at 2-second intervals, resulting in a maximum rate of phase change of 0.12 cycles per sample. In fact, for any sampled waveform with negligible energy above the Nyquist frequency, the rate of phase change is less than 0.5 cycle per sample, as long as the reference frequency is lower than the Nyquist frequency. This means that, in order to obtain the true phase values, we must eliminate phase 'discontinuities' greater than π radians, by either adding or subtracting 2π radians at those 'discontinuities':

$$\phi(t_i) = \phi(t_i) + 2\pi \quad , \qquad \phi(t_i) - \phi(t_{i-1}) \leq -\pi \quad ; \qquad \text{(II-9a)}$$

$$\phi(t_i) = \phi(t_i) - 2\pi \quad , \qquad \phi(t_i) - \phi(t_{i-1}) > \pi \quad . \qquad \text{(II-9b)}$$

We call the resulting phase time series the 'continuous' phase.

The instantaneous frequency is defined as the time derivative of the 'continuous' instantaneous phase:

$$f(t) = \frac{1}{2\pi} \frac{d\phi(t)}{dt} + f_o \, . \qquad \text{(II-10)}$$

In our algorithm, we take first differences of the 'continuous' phase, rather than performing an n-point numerical differentiation, since we do not want to smooth the data when searching for the onset of signals.

The Hilbert transform is performed with a 'fast' Hilbert transform algorithm given by Čiček (1970); this algorithm has been programmed and described also by Shen (1974). Alternative methods include n-point recursive

algorithms; these, however, probably also impose waveform bandwidth limitations which we prefer to avoid at this point in the development.

C. AMPLITUDE AND PHASE DETECTION THEORY

The vector diagrams in Figure II-2 illustrate how the instantaneous value of a received waveform is determined by the interaction of a signal vector $\vec{s}(t)$ and a noise vector $\vec{n}(t)$, combining to the resultant waveform vector $\vec{r}(t)$ with modulus or instantaneous amplitude $|\vec{r}(t)|$ and angular argument or instantaneous phase $\phi(t)$. Without loss of generality the signal phase is assumed zero; the noise phase, $\phi_n(t)$, can have any value within a 2π interval, as indicated by the dotted circle.

Let us now investigate the envelope and phase detection potential.

1. *Envelope Detection*

Envelope (instantaneous amplitude) detection by an analyst usually requires that in a presumed signal gate the envelope, $|\vec{r}_s(t)|$, is greater than the maximum envelope, $|\vec{n}|_{max}$, in a lagging, presumed noise gate. However, the vector diagrams show that even when, at a given instant, the signal-to-noise ratio (SNR) is greater than one but less than two, the instantaneous waveform amplitude is not necessarily greater than the instantaneous noise amplitude $|\vec{n}(t)|$, and certainly not necessarily greater than $|\vec{n}|_{max}$. The chance that, for an instantaneous SNR of less than 6 dB, the waveform envelope is greater than $|\vec{n}|_{max}$ depends on the noise phase angle, relative to the signal phase. Thus, to determine if a signal is present, it is probably best to count the number of times that $|\vec{r}_s(t)| > |\vec{n}|_{max}$. For a sufficient number of observations N (i.e., a sufficiently long presumed signal gate) this count, divided by N, approximates the probability $P(|\vec{r}_s(t)| > |\vec{n}|_{max})$.

To get some insight in the envelope detector performance using the above detection criterion, we consider, ensemble-wise, the probability

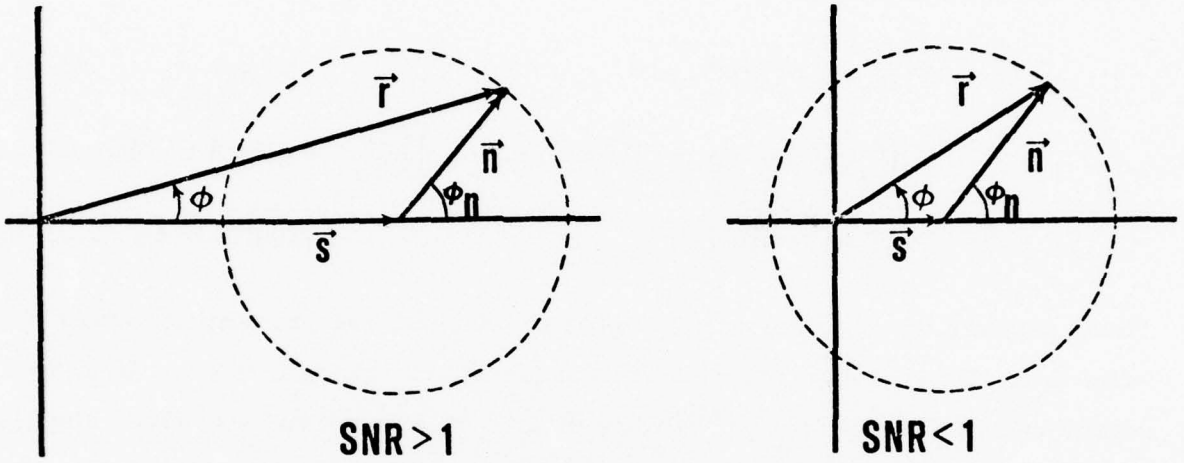

$|\vec{r}|$ = instantaneous amplitude

ϕ = instantaneous phase

FIGURE II-2

VECTOR DIAGRAM REPRESENTATION OF SIGNAL AND NOISE INTERACTION

that at a given instant, t, for a given instantaneous SNR, $|\vec{s}(t)|/|\vec{n}(t)|$, the instantaneous waveform amplitude is greater than the instantaneous noise amplitude, $P(|\vec{r}_s(t)| > |\vec{n}(t)|)$. This probability can be derived from vector diagram geometry (Appendix B), and turns out to be a well-behaved function of the instantaneous SNR:

$$P(|\vec{r}_s(t)| > |\vec{n}(t)| = 0 \quad , s(t) = 0 \tag{II-11a}$$

$$P(|\vec{r}_s(t)| > |\vec{n}(t)| = 1 - \pi^{-1} \arccos \frac{|\vec{s}(t)|}{2|\vec{n}(t)|} \quad , 0 < |\vec{s}(t)| \leq 2|\vec{n}(t)| \tag{II-11b}$$

$$P(|\vec{r}_s(t)| > |\vec{n}(t)| = 1 \quad , |\vec{s}(t)| \geq 2|\vec{n}(t)| . \tag{II-11c}$$

Thus, already when a very small signal is present, the probability jumps to the value 0.5. This probability distribution function is given in Figure II-3, together with the phase bias probability distribution curve to be derived shortly.

Since we cannot measure the instantaneous noise amplitude when a signal is present in the presumed signal gate, we cannot use $|\vec{r}(t)| > |\vec{n}(t)|$ as a detection criterion. However, we can relate the probability that the analyst's detection criterion, $|\vec{r}(t)| > |\vec{n}|_{max}$, is satisfied, to the probability function of Equation (II-11). This relationship is not very rigorous but improves our insight in envelope detection sensitivity. If we set a threshold, n_o, such that, most of the time, $|\vec{n}(t)| < n_o$, then

$$P(|\vec{r}_s(t)| > n_o) < P(|\vec{r}_s(t)| > |\vec{n}(t)|). \tag{II-12}$$

If, for instance, we set $n_o = |\vec{n}|_{max}$ as in the analyst's method, it follows that

$$P(|\vec{r}_s(t)| > |\vec{n}|_{max} = \epsilon \quad , \quad s(t) = 0 \tag{II-13a}$$

$$\epsilon < P(|\vec{r}_s(t)| > |\vec{n}|_{max}) < 1 - \pi^{-1} \arccos \frac{|\vec{s}(t)|}{2|\vec{n}(t)|} \quad , \quad 0 < |\vec{s}(t)| \leq 2|\vec{n}(t)| \tag{II-13b}$$

$$\epsilon < P(|\vec{r}_s(t)| > |\vec{n}|_{max}) < 1 \quad , \quad |\vec{s}(t)| \geq 2|\vec{n}(t)| \quad , \tag{II-13c}$$

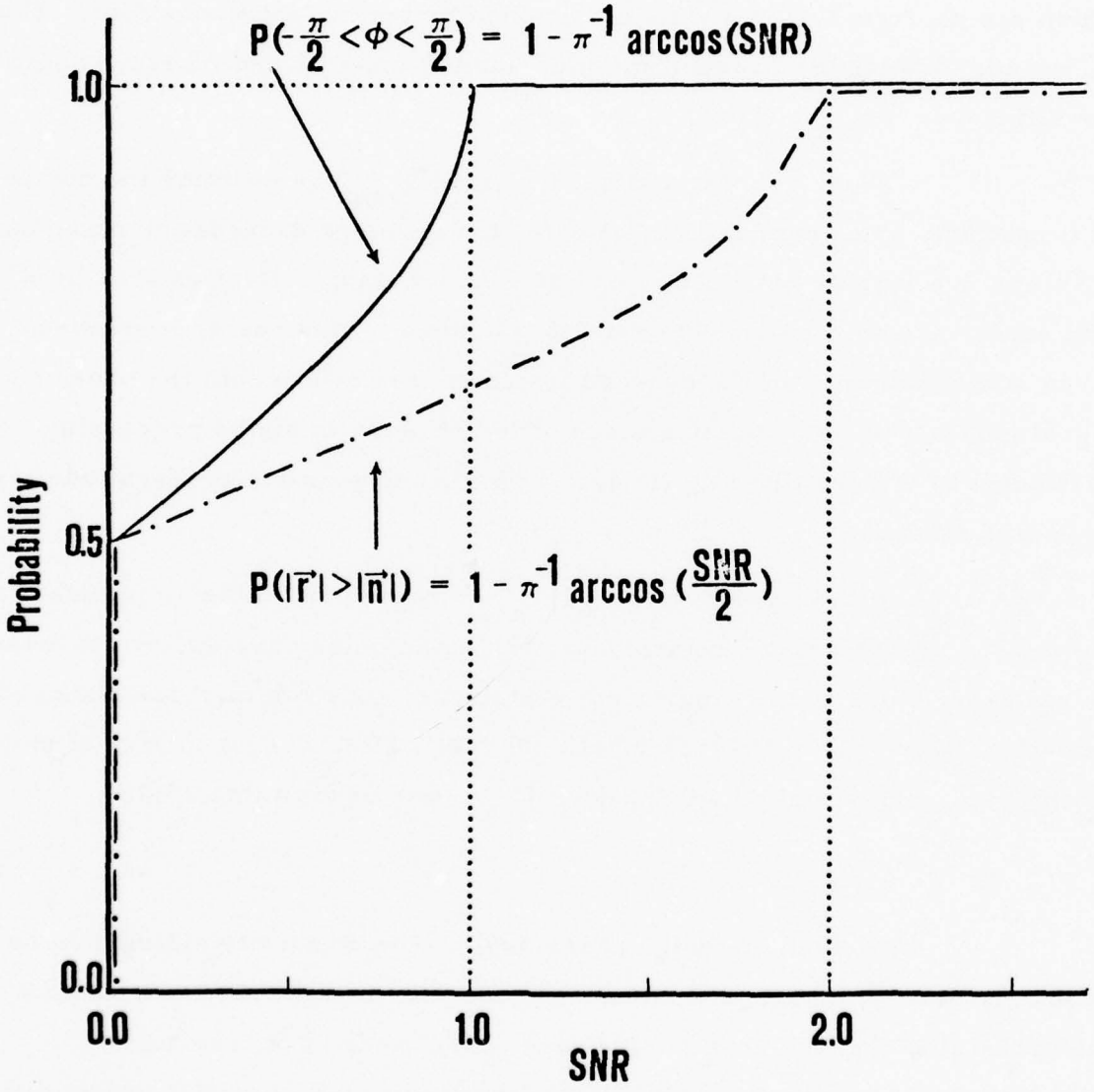

FIGURE II-3

ENVELOPE AND PHASE PROBABILITY
DISTRIBUTION CURVES

where the small value ϵ is the probability that, in the absence of signal, the envelope in the presumed signal gate is greater than the maximum envelope in the lagging, presumed noise gate. This value depends on the statistical distribution of noise envelope values. In the presence of signal, $P(|\vec{r}_s(t)| > |\vec{n}|_{max})$ is greater than ϵ, and increases with SNR, but is subject to an upper bound which ranges from 0.5 to 1.0 as determined by the instantaneous SNR. The difference between the probability value and the upper bound increases with the difference $|\vec{n}|_{max} - |\vec{n}(t)|$.

Thus, approximating $P(|\vec{r}_s(t)| > |\vec{n}|_{max})$ by counting the number of times that, in a presumed signal gate, the envelope exceeds the maximum envelope in a lagging noise gate, and setting a suitable detection threshold for this count, seems a reasonable detection method. This count, moreover, gives some indication of the average instantaneous SNR within the presumed signal gate. This is a valuable piece of information in signal processing, in particular in Wiener filtering (Unger, 1976b), and possibly in magnitude bias reduction methods.

Instead of the value $|\vec{n}|_{max}$, any other suitable amplitude threshold may be used such as, for instance, the mean noise envelope or the mean log noise envelope, or its equivalent z-statistic, plus two or three standard deviations (Sax et al., 1974; Swindell and Snell, 1977). As a matter of simplicity, the analyst criterion $|\vec{r}(t)| > |\vec{n}|_{max}$ was used in this study.

2. Phase Detection

Assume the noise phase angle to be uniformly distributed between $-\pi$ and $+\pi$ radians. Then, for a waveform consisting of noise only, the probability that the phase is between $-\pi/2$ and $+\pi/2$ radians, $P(|\phi(t)| < \pi/2)$, equals 0.5. The vector diagrams in Figure II-2 and Appendix B show that, when a signal is present, the phase angle is statistically biased, i.e., the above probability is greater than 0.5. For a given instantaneous SNR, this probability is (Appendix B):

$$P(|\phi(t)| < \pi/2) = 0.5 \quad , \quad s(t) = 0 \qquad \text{(II-14a)}$$

$$P(|\phi(t)| < \pi/2) = 1 - \pi^{-1} \arccos \frac{|\vec{s}(t)|}{|\vec{n}(t)|} \quad , \quad |\vec{s}(t)| \leq |\vec{n}(t)| \qquad \text{(II-14b)}$$

$$P(|\phi(t)| < \pi/2) = 1 \quad , \quad |\vec{s}(t)| > |\vec{n}(t)| \; . \qquad \text{(II-14c)}$$

For a constant SNR, this phase bias probability can be approximated by counting, within a waveform window of sufficient length, the number of times that the phase fluctuation is within $\pm \pi/2$ radians, and dividing this count by the number of window points. However, since in general the SNR will vary inside the window, this approximated phase bias probability will not relate to the SNR exactly as in Equations (II-14). Nevertheless, it still is some measure of the average SNR in the window, and is a good detection parameter, since it will have a value greater than 0.5 if a signal is present in the window. In this manner, phase detection is established in principle. In the application to actual data, however, there are some complications which will be discussed shortly.

The phase bias probability distribution function is compared to the envelope detection probability distribution function in Figure II-3. We observe the important fact that the phase distribution curve reflects a detection sensitivity which is twice that of the envelope, since the arccosine argument equals the instantaneous SNR in the case of phase detection, and only one half the instantaneous SNR in the case of envelope detection. This suggests that, in principle, phase detection is at least 6 dB better than envelope detection, especially when regarding the fact that the envelope curve represents the upper bound of envelope detection sensitivity. The detection sensitivity of the instantaneous phase has been shown and used, for instance, in underwater sound propagation studies (Steinberg and Birdsall, 1966; Unger and Veenkant, 1967a, 1967b). In this study we attempt to apply it to the detection and timing of seismic signals.

Since, in general, the signal phase varies with time in a deterministic manner (e.g., in LP dispersed waveforms), the principle of phase detection can only be applied in those cases where a model for the expected signal phase angle variations can be adequately specified. As will be discussed in the next section, such a model can be specified for most LP waveforms, but not for most SP waveforms. Also, contrary to our assumption above, the noise phase is not uniformly distributed, but may rather follow a somewhat more deterministic trend. This is the case, for instance, when the dominant noise frequency differs from the reference frequency, f_o, thus causing a linear phase trend. The 'continuous' phase then may traverse a number of cycles within a given time gate. These facts necessitate 'tracking' the instantaneous phase function; the phase fluctuations about the tracked or time-variant mean phase then may be studied for signal detection. For noise, the fluctuations should be randomly distributed; in the presence of signal they will be statistically biased. Thus, the performance of the phase detector now rests with the efficiency of the phase tracking process with respect to some presumed model governing the phase variations of signals, and also with the validity of that model used to estimate the signal phase angle.

One method of phase tracking is moving-window quadratic regression on the time series of the 'continuous' phase (Appendix A). For each window, the mean-square error or phase standard deviation (s.d.), and the phase bias probability, $P(|\phi - \hat{\phi}| < \pi/2)$, where $\hat{\phi}$ is the regressed phase within a window, are measures of the amount of phase fluctuation. Again, this probability can be approximated by counting, in a sufficiently large window, the number of times that the phase fluctuation about the time-variant mean phase is within $\pm\pi/2$ radians, and dividing this count by the number of window data points. This probability also is a measure of the average SNR in the window, provided that the phase regression model adequately describes the waveform's phase over the duration of the window. Sudden frequency changes in noise and/or signal, for example, would distort this measure.

One now may set suitable detection thresholds for both the phase s.d. (e.g., $\pi/2$), and the phase bias probability (e.g., 0.8). A signal detection then is declared when for a certain window the phase s.d. falls below the threshold, and the phase bias probability exceeds its threshold. The window start time for the window with minimum phase s.d. or maximum phase bias probability should be close to the signal onset time. These minima and maxima become especially sharp when the first and second order coefficients in the quadratic phase regression polynomial are known, for instance, for a priori known,near-linear LP signal dispersion.

The envelope and phase detection criteria, derived above from vector diagram geometry, form the basis for the design of the automatic detection and timing algorithms described in Section III.

3. Detection and Timing of Early Secondary Signals

In previous work (Farnbach, 1975; Unger, 1976a) it was shown that the instantaneous amplitude, phase, and frequency may be used in determining the onset of early secondary SP signals such as pP. The arrival of such signals rapidly changes the waveform vector in either modulus or argument, or in both; these changes are measurable in the time series of the instantaneous amplitude, phase, and frequency. The rate of change in these parameters depends on the arrival time delay of the secondary signal relative to the primary signal arrival, on its amplitude and phase, its rise time, the noise condition during its arrival, and the amplitude and the decay function of the primary signal. For a very short rise time, and a sizeable relative amplitude of the secondary signal, the change in amplitude and phase approaches a step function. By differentiation, this phase change turns into a spike in the instantaneous frequency.

The detection and timing of pP signals can be instrumental in the discrimination between earthquakes and nuclear explosions. For shallow,

supposedly point source events, the pP signals are expected to arrive within 0.4 to 0.9 seconds after the primary signal, independent of propagation path, but dependent on source depth and medium. This has been confirmed with cepstrum analysis (e.g., Lane and Sun, 1975; Sun, 1975). Similar secondary signal delays were measured with the instantaneous amplitude, phase, and frequency for several presumed nuclear explosions in eastern Kazakh (Unger, 1976a). For earthquakes, the earliest secondary signals usually arrive later than one second after the primary signal.

The behavior of early secondary signals is studied in Sections IV and V.

SECTION III

AUTOMATIC SP AND LP SIGNAL DETECTION AND TIMING ALGORITHMS

A. INTRODUCTION

The envelope and phase detection theory, developed in the previous section, is now applied in the design of SP and LP automatic signal detection and timing algorithms. The designs are furthermore based on a study of signal characteristics, leading to the conclusion that SP signals in general require envelope detection, but that LP signals are most conveniently detected and timed with moving-window phase regression.

B. SP SIGNAL DETECTION AND TIMING

1. Background

A study of SP waveforms indicated that, in general, some secondary signals arrive within one to two seconds after the main signal. This means that, at a 10-Hz sample rate, less than 10 to 20 points are available for phase regression in one window; this is insufficient for meaningful results. Longer windows would contain sharp phase changes due to these early secondary arrivals; these sharp changes would render the phase regression results useless for the detection and direct timing of the main signal arrival. However, as will be shown later, the phase information is used in the timing of the early secondary signals, and may also be useful in seismic discrimination. Moreover, the instantaneous frequency, derived from the instantaneous phase, is used indirectly in the timing of main SP signal arrivals.

The inability to perform a meaningful regression analysis on the SP phase function makes us resort to the method of envelope detection

and timing. The SP signal detection and timing procedure, outlined below, closely follows that of an analyst, by searching for the start of the first signal period after a detection has been declared.

2. Procedure

The procedure of detecting and timing the onset of SP signals is as follows (Figure III-1). First, over a specified warm-up period (e.g., 40 seconds), the peak noise envelope, $|\vec{n}|_{max}$, is established. This peak envelope is cosine tapered over subsequent waveform points, with a specified time constant (e.g., with a 60-second time constant, the original peak value is halved at 30 seconds and equals zero at 60 seconds). An envelope value exceeding the tapered peak value establishes a new noise peak, unless a signal detection is declared; in that case no noise peak update takes place until the signal is declared to be terminated.

A signal detection is called whenever, in a forward looking (leading) time window of specified length (e.g., 4 seconds), the probability that the envelope is greater than the tapered peak noise envelope, $P(|\vec{r}_s(t)|>|\vec{n}|_{max})$ exceeds a specified threshold, TH1 (e.g., TH1 = 0.3). When this probability reaches its maximum the algorithm starts looking for the first signal envelope peak. When the ratio of first signal envelope peak and tapered noise envelope peak exceeds a second specified threshold, the SNR threshold TH2 (e.g., TH2 = 2 to 3 dB), the signal detection is confirmed and a frequency-dependent stepback is performed to determine the signal onset time.

The stepback procedure (Figure III-2) is based on the observation that in most cases the first signal envelope peak (at t_4) occurs within one signal period, and frequently at approximately 3/4 period, after the signal onset (at t_0). In a high-SNR waveform the signal onset time is most accurately found by detecting the first maximum or minimum of the signal's instantaneous value (at t_3), and stepping back 1/4 period (=0.25/instantaneous frequency at t_3).

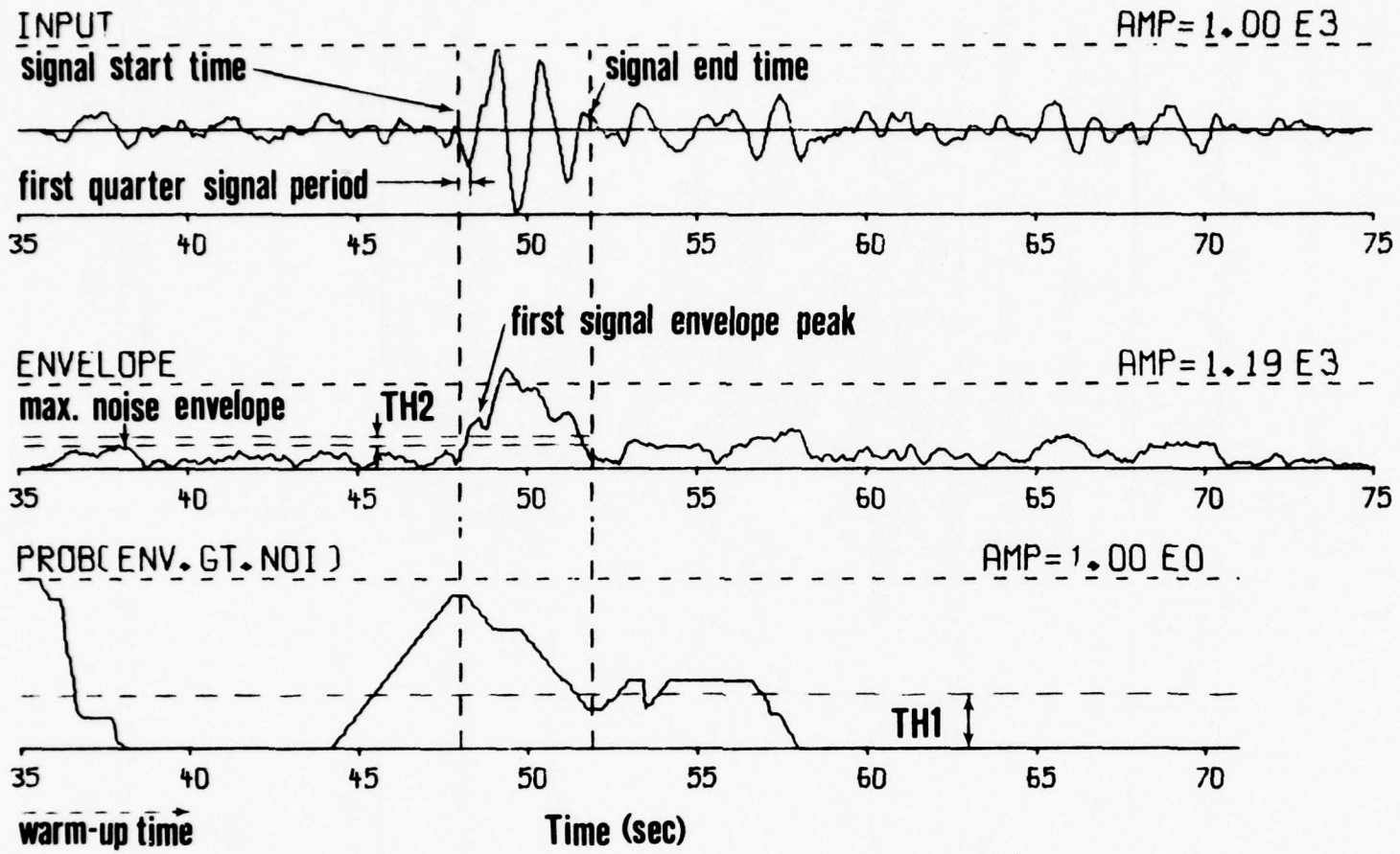

FIGURE III-1

SF SIGNAL DETECTICN AND TIMING

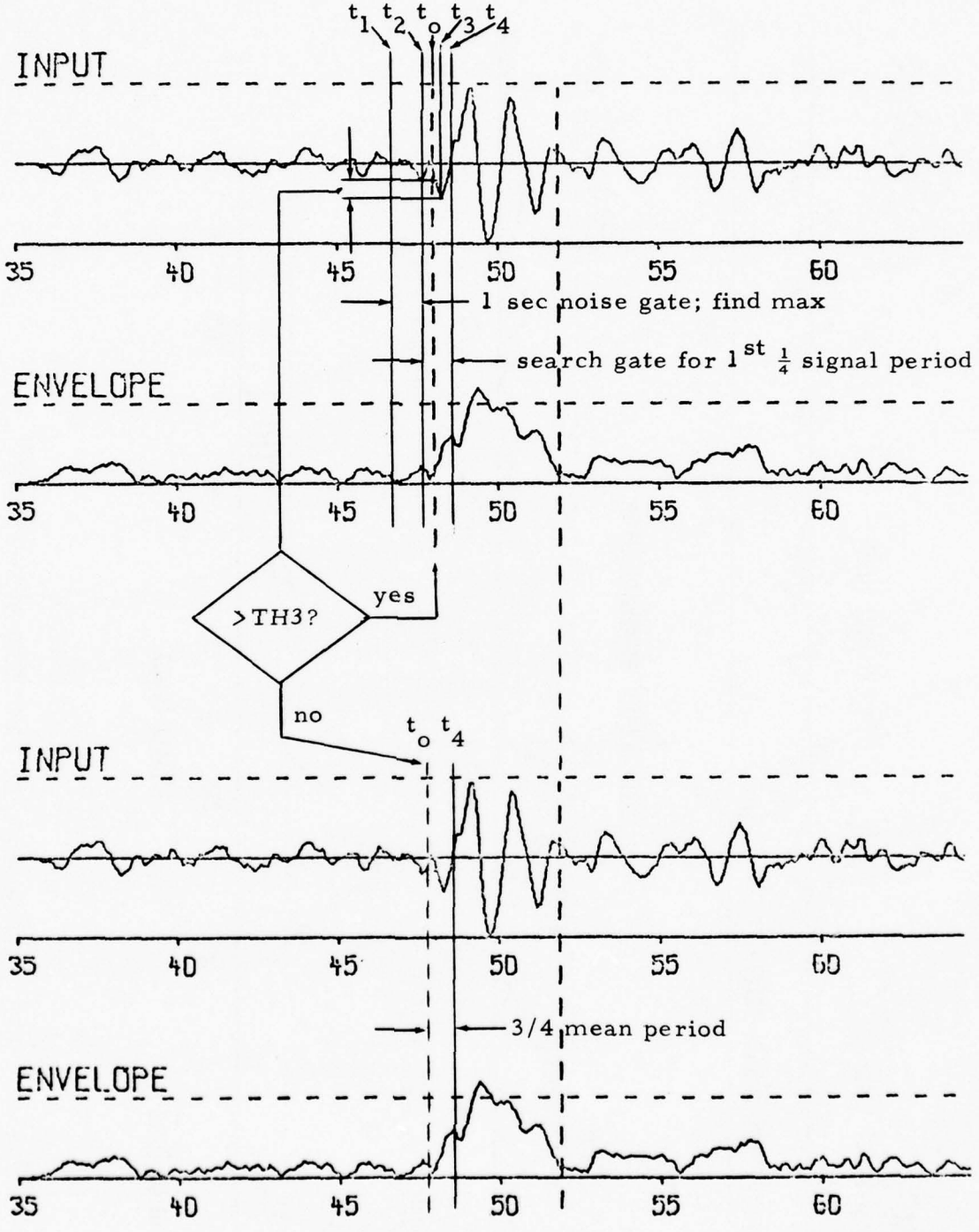

FIGURE III-2

STEPBACK PROCEDURE IN SP SIGNAL TIMING

For low-SNR waveforms the first quarter period may be obscured by noise; in that case we step back 3/4 mean period (=0.75/mean frequency at t_4) from the first signal envelope peak at t_4. The mean frequency is the closed-form derivative of the phase regression polynomial evaluated at time t_4 (Appendix A). The search for the first quarter period is started at t_2, i.e., at 0.8 mean period before t_4; the first quarter period is detected when its maximum or minimum exceeds, by a third threshold, TH3 (e.g., TH3= 1 dB), the immediately preceding noise in the one-second time interval (t_1, t_2).

If the second threshold (the SNR threshold) is not satisfied, the detection is annulled and the noise peak value is updated with what at first was believed to be the signal envelope peak. Thereafter, the noise peak is updated as usual, until the next supposed signal detection, etc.

The signal end time is found as the moment of the first envelope *minimum* occurring either after $P(|\vec{r}_s(t)| > |\vec{n}|_{max})$ falls below its threshold, or after the signal duration exceeds a specified maximum, whichever is first. If this envelope minimum is greater than the tapered noise peak the noise peak envelope is updated with this value, and noise peak updating and signal detection resume as normal. In principle this procedure enables the detection and timing of later phases and other signals in the coda.

The above procedure is not necessarily the best, but was arrived at after rather extensive study of typical SP waveforms. It seemed to respond well to a limited set of NORSAR single-site waveforms. The algorithm's performance, and some possible alternative methods, are discussed in Section IV.

C. LP SIGNAL DETECTION AND TIMING

1. Background

The early, low-frequency, parts of LP signals, in general, do not contain secondary signal arrivals, and establish well-defined, near-linear dispersion curves (Unger, 1976b). These facts, and the relatively long

duration of these waveform parts make them very suitable for detection and timing by moving-window phase regression. Moreover, since a prime application of LP signal timing is time-variant Wiener filtering along regionally known dispersion curves (Unger, 1976b) the linear dispersion information in that case can be input as a priori known first and second order coefficients in the phase regression polynomial. With the emphasis on this application, and because phase detection was shown to be in principle 6 dB more sensitive than envelope detection, we focused on phase detection for LP signals, and did not further consider LP envelope detection.

The LP moving-window phase regression detection and timing procedure is outlined below.

2. Procedure

Automatic LP signal detection and timing are performed with a moving-window quadratic regression analysis on the 'continuous' instantaneous phase time series, exactly as described in Section II and, in more detail, in Appendix A. With the emphasis on the time-variant Wiener filtering application, for which the start of a known dispersion curve must be obtained, this dispersion information is input as the a priori known, and constant first and second order coefficients in the quadratic phase regression polynomial. This results in a sharp minimum in the phase s.d., and a strong maximum in the phase bias probability, when the regression window fits the signal dispersion curve (Figure III-3). If the phase s.d. minimum is below a specified threshold (e.g., $\pi/2$ radians), and the phase bias probability maximum is above its specified threshold (e.g., 0.8), a signal detection is declared, and the signal onset time is taken to be the time of occurrence of the phase s.d. minimum. The values of the phase s.d. minimum and the phase bias probability maximum supposedly are an indication of the goodness-of-fit in the regression, and therefore, possibly also of the size of the timing error, and of the average SNR in the window. Since LP signal dispersion is in general

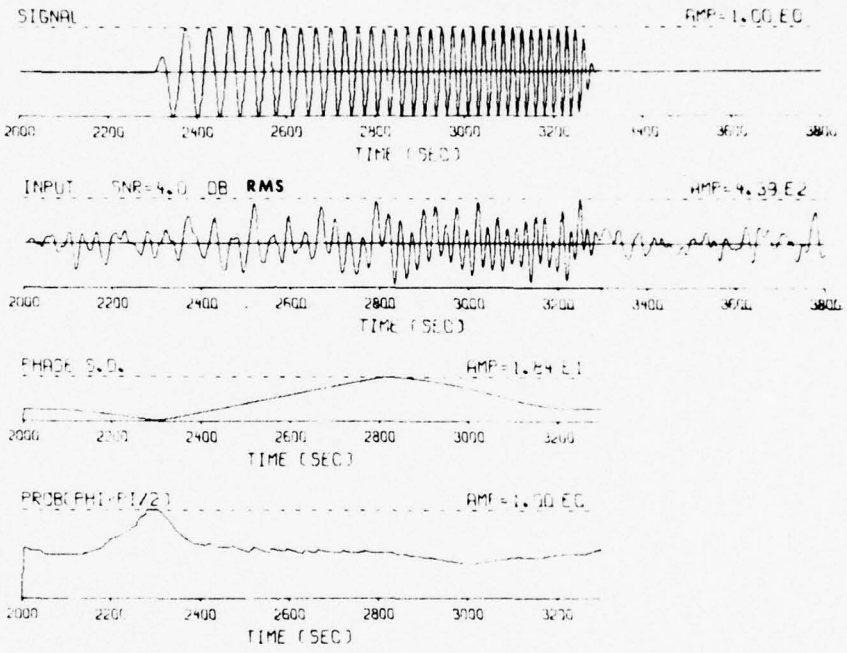

FIGURE III-3

AUTOMATIC LP SIGNAL DETECTION AND TIMING BY MOVING-WINDOW PHASE REGRESSION

not well defined in the higher frequencies (0.035 to 0.060 Hz), the window length specified should cover only the lower signal frequencies (0.015 to 0.035 Hz). These frequency boundaries may vary for different station-region pairs.

The performance evaluation of the automatic LP signal detector and timer is discussed in Section IV.

SECTION IV
EVALUATION

A. INTRODUCTION

The automatic SP and LP signal detection and timing algorithms were evaluated by application to real and simulated data. The evaluation results are described and discussed below.

B. EVALUATION OF THE SP SIGNAL DETECTION AND TIMING ALGORITHM

1. Evaluation

The automatic SP signal detection and timing algorithm, described in Section III, was evaluated by application to a small data base consisting of digitized NORSAR single-site SP seismograms. This data base, listed in Tables IV-1 and IV-2 was also used previously in a demonstration of seismic event discrimination by interactive processing (Sax, 1976). The data base contains the signals, and 35 to 50 seconds of preceding noise, of 20 shallow Eurasian earthquakes, ranging in magnitude from $m_b = 4.5$ to $m_b = 6.1$ and in epicentral distance from 24.8° to 76.0°; nine presumed nuclear explosions in eastern Kazakh (EKZ); two Russian presumed peaceful nuclear explosions (PNE); three presumed nuclear explosions at the U.S. Nevada Test Site (NTS); one presumed peaceful nuclear explosion in Colorado.

This data base seems to provide a reasonably large variety of signal characteristics and as such is suitable for an initial evaluation of the automatic detector/timer algorithm. However, the data set may not be typical in the sense of signal strength, i.e., it contains a relatively high number

TABLE IV-1

EARTHQUAKE DATA BASE
(PAGE 1 OF 2)

Event Number	Classification **	m_b	Depth (km)*	Distance (degrees)	Azimuth	Latitude (^oN)	Longitude (^oE)	Date	Origin Time
01	Q	5.1	55	63.9	19.7	52.8	160.8	06/15/71	14:04:08.0
02	Q	5.2	N	44.1	84.0	41.5	78.3	06/19/71	17:23:02.0
04	Q	5.6	20	65.3	23.3	50.4	156.8	08/01/71	02:16:04.1
06	Q	4.6	N	32.7	116.6	38.1	49.1	05/15/71	04:53:05.5
14	Q	5.4	16	55.4	87.7	30.8	84.5	05/03/71	00:42:13.3
17	Q	4.8	N	61.6	16.9	55.6	163.9	01/12/72	20:20:15.0
20	Q	5.0	N	48.1	88.2	36.5	78.5	08/29/71	15:16:56.0
21	Q	6.1	29	65.3	35.0	46.7	141.4	09/06/71	13:37:11.0
22	Q	6.0	7	69.9	29.2	44.4	150.9	09/09/71	23:01:06.0
26	Q	4.5	9	24.8	143.0	39.0	29.8	10/05/71	18:53:06.0

* N - Not Given
** Q - Eurasian Earthquake

TABLE IV-1

EARTHQUAKE DATA BASE
(PAGE 2 OF 2)

Event Number	Classification **	m_b	Depth (km)*	Distance (degrees)	Azimuth	Latitude (^oN)	Longitude (^oE)	Date	Origin Time
30	Q	4.5	27	25.1	155.4	37.1	24.0	02/13/72	13:07:10.5
31	Q	4.9	17	44.5	83.3	41.3	79.3	07/03/71	04:33:49.1
38	Q	5.5	23	44.9	86.2	31.4	91.5	02/11/72	05:55:46.0
44	Q	4.7	N	59.4	77.1	32.6	95.8	07/16/72	03:40:00.0
48	Q	4.8	N	56.2	162.9	56.2	162.9	07/31/72	06:40:28.0
55	Q	5.4	31	40.4	121.0	30.1	50.8	07/02/72	12:56:07.0
57	Q	4.8	N	49.5	87.3	35.8	80.6	07/24/72	15:06:19.8
87	Q	5.9	28	76.0	40.0	35.0	141.2	01/20/75	17:31:10.6
89	Q	5.7	7	74.3	48.5	33.2	131.3	04/20/75	17:35:50.4
90	Q	5.8	24	74.3	38.5	37.1	142.1	05/04/75	09:31:59.5

* N - Not Given
** Q - Eurasian Earthquake

TABLE IV-2

PRESUMED EXPLOSION DATA BASE

Event Number	Classification **	m_b	Depth (km)	Distance (degrees)	Azimuth	Latitude (^oN)	Longitude (^oE)	Date	Origin Time
07	E	5.4	0	38.0	74.7	50.1	79.1	06/30/71	03:56:57.2
13	E	5.5	0	37.4	75.9	50.0	77.7	06/06/71	04:02:57.1
16	E	4.7	0	37.5	76.0	49.9	77.6	12/07/74	05:59:56.9
49	E	5.1	0	37.4	75.9	50.0	77.7	09/02/72	08:56:58.0
51	E	5.2	0	37.8	75.8	49.8	78.1	08/16/72	03:16:57.2
53	E	6.0	0	37.9	74.9	50.1	78.8	12/10/72	04:27:08.4
56	E	4.4	0	37.8	76.0	49.7	78.0	07/06/72	01:02:58.0
58	E	5.7	0	37.8	75.8	49.8	78.1	12/10/72	04:26:57.7
77	E	4.7	0	37.2	75.7	49.9	78.1	06/25/74	03:56:57.6
32	P	5.2	0	35.8	88.8	45.6	67.9	09/13/73	02:59:57.2
60	P	5.3	0	37.7	92.6	42.7	67.4	08/15/73	01:59:58.0
11	N	5.8	0	72.9	318.4	37.2	-116.0	08/30/74	15:00:00.0
15	N	5.5	0	73.0	318.4	37.1	-116.0	07/08/71	14:00:00.0
81	N	5.6	0	72.9	318.4	37.2	-116.0	07/26/74	15:05:00.2
59	C	5.4	0	68.0	313.9	39.8	-108.4	05/17/73	16:00:00.0

** E - Eastern Kazakh Presumed Nuclear Explosion
P - Russian Presumed Peaceful Nuclear Explosion
C - Colorado Presumed Peaceful Nuclear Explosion
N - Nevada Test Site Presumed Nuclear Explosion

of high SNR waveforms. Also, the frequency content of both noise and signal may be different at other stations; this may require adaptation of the signal detection and timing algorithms to the characteristics prevailing at those stations. Therefore, the detection results should not be interpreted as typical operating characteristics. Determining the true operating characteristics of a newly designed detector is a complex task, in part also due to the general lack of a good detection and false alarm reference. Moreover, this would require a high amount of processing which could not be provided for in the present study. Nevertheless, the results demonstrate the feasibility of, and establish a trend of detection ratio versus false alarm rate for the automatic detector, and provide initial performance characteristics for the automatic timer.

The evaluation results are presented in Figures IV-1, IV-2, and IV-3, and in Table IV-3. Figure IV-1 presents the relevant waveform parts with both automatic and suggested analyst timing. Figure IV-2 gives the detection versus false-alarm statistics for this particular data set. Table IV-3 shows the threshold settings used in the detection evaluation. Figure IV-3 gives the timing error statistics.

In four out of the 35 available waveforms no signal could be detected by the analyst. In one of the waveforms two signals were present (event 53); both were used in the timing evaluation, but only the first one was used in the detection evaluation. In two of the 31 analyst detections (events 56, 16) the signal was below surrounding noise peaks, but could be detected by a change in waveform characteristics. These two signals and one emergent signal (event 01) were missed by the automatic detector, even at the lower threshold settings. For 25 analyst detections (including the second signal in the waveform of event 53) it was believed that the signal onset time could be picked by the analyst with 0.1-sec accuracy; the automatic timing results for these waveforms are reflected in the solid histogram bars in Figure IV-3a. For three analyst detections (events 44, 30, and 38), two of them emergent (events 30, 38), the onset time could not be determined accurately by the analyst; the

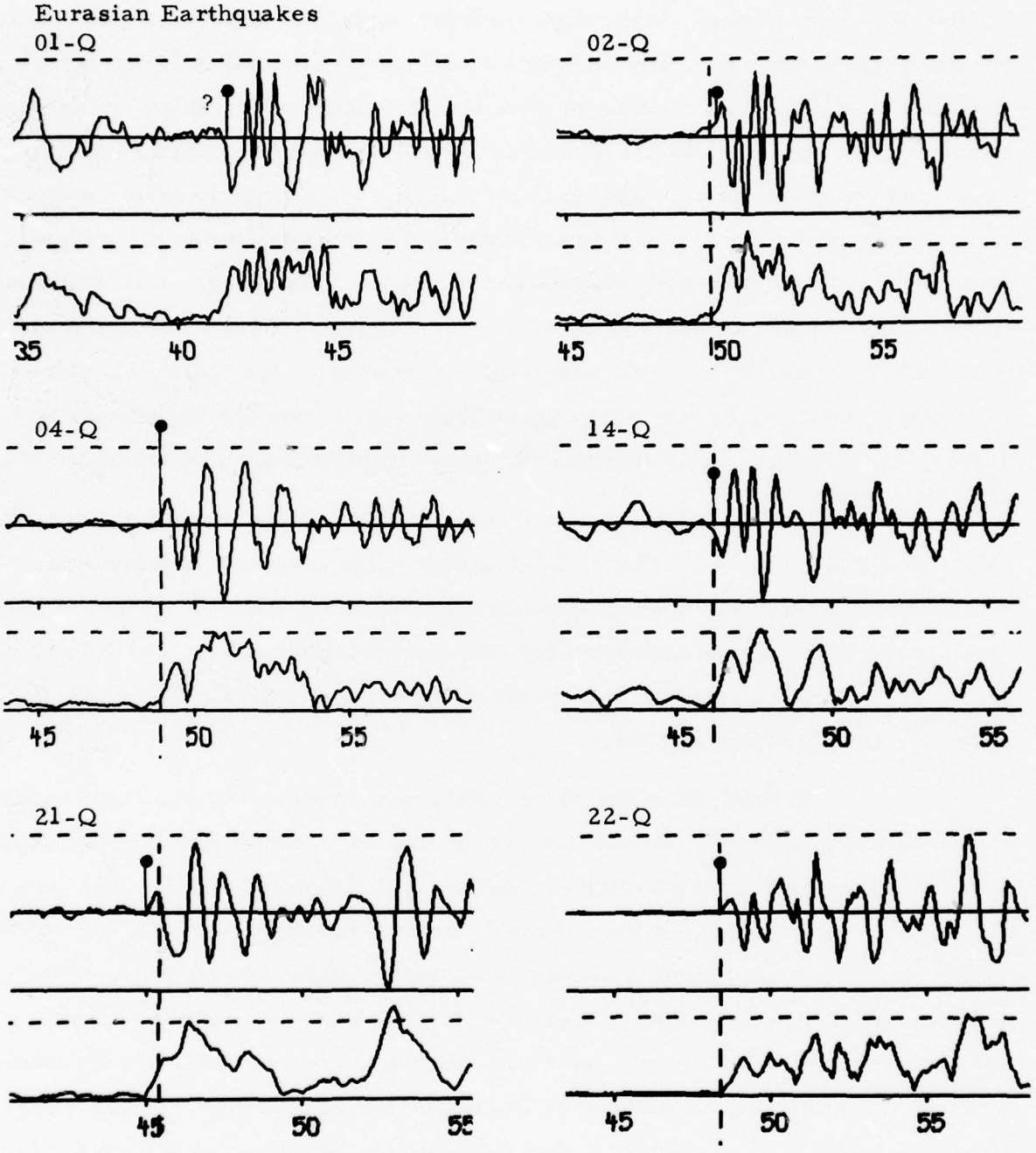

FIGURE IV-1

AUTOMATIC (¦) VERSUS ANALYST (🡑) SIGNAL TIMING
(PAGE 1 OF 6)

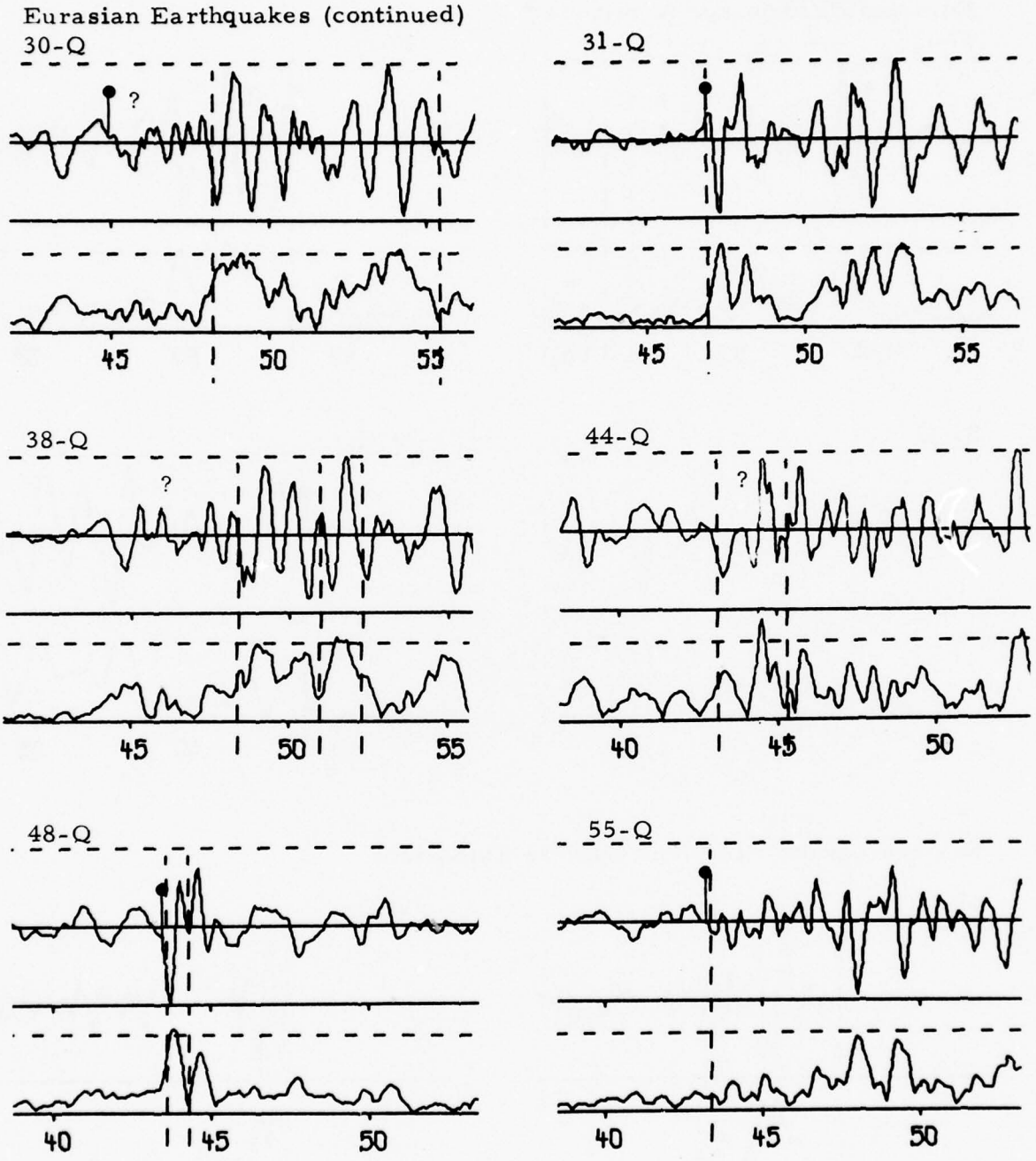

FIGURE IV-1

AUTOMATIC (┆) VERSUS ANALYST (📍) SIGNAL TIMING
(PAGE 2 OF 6)

Eurasian Earthquakes (continued)

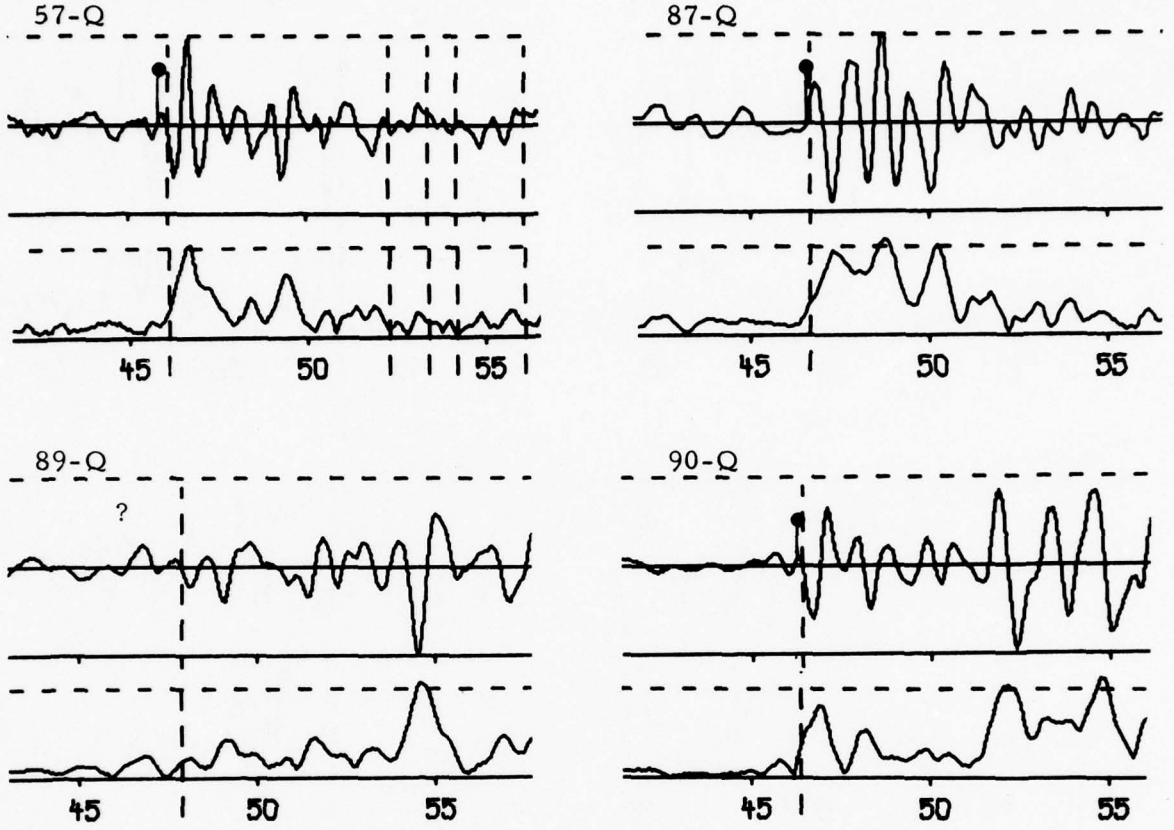

Eastern Kazakh Presumed Nuclear Explosions

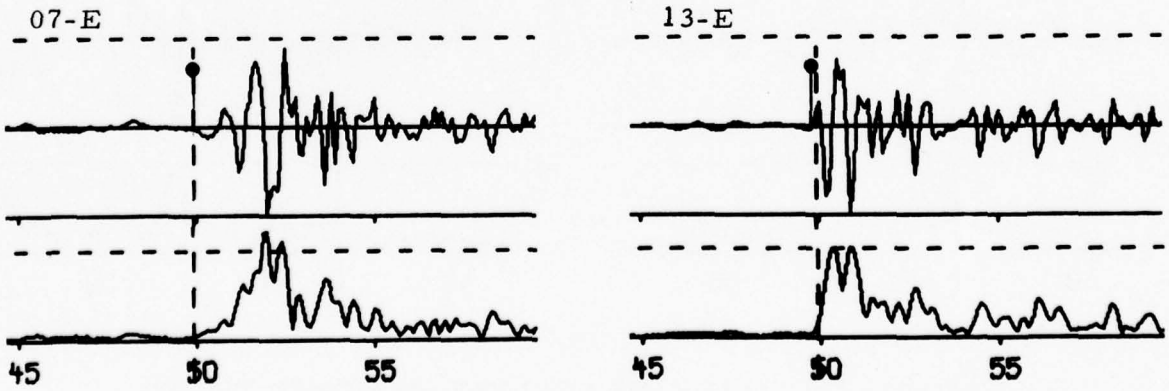

FIGURE IV-1

AUTOMATIC (┆) VERSUS ANALYST (🡇) SIGNAL TIMING
(PAGE 3 OF 6)

Eastern Kazakh Presumed Nuclear Explosions (continued)

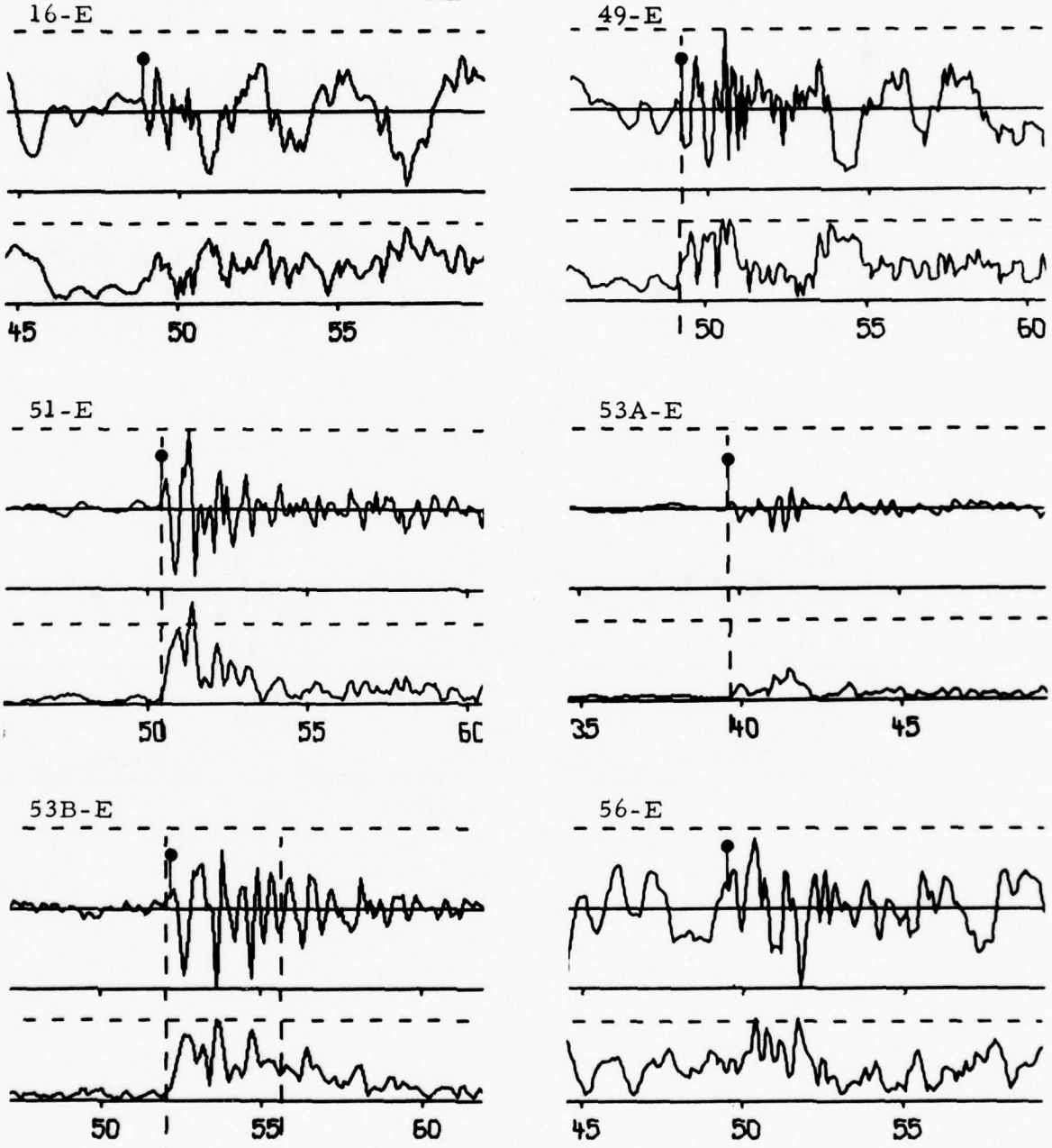

FIGURE IV-1

AUTOMATIC (¦) VERSUS ANALYST (•) SIGNAL TIMING
(PAGE 4 OF 6)

Eastern Kazakh Presumed Nuclear Explosions (continued)

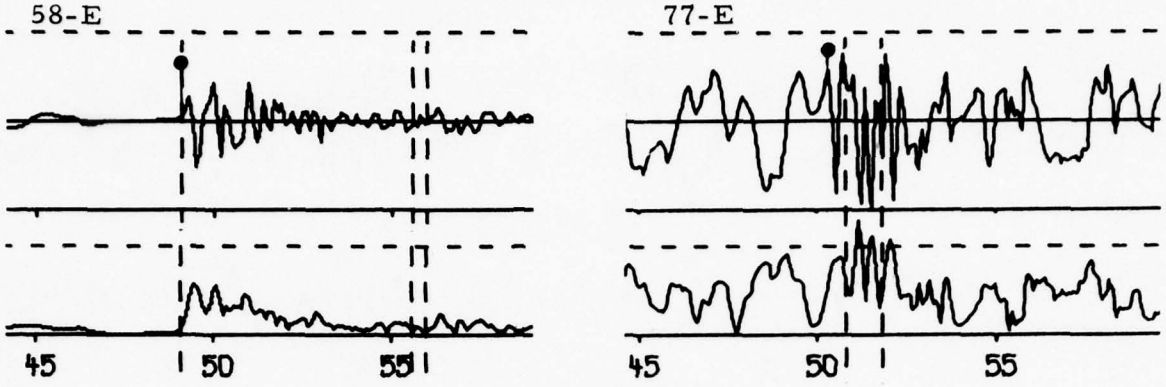

Russian Presumed Peaceful Nuclear Explosions

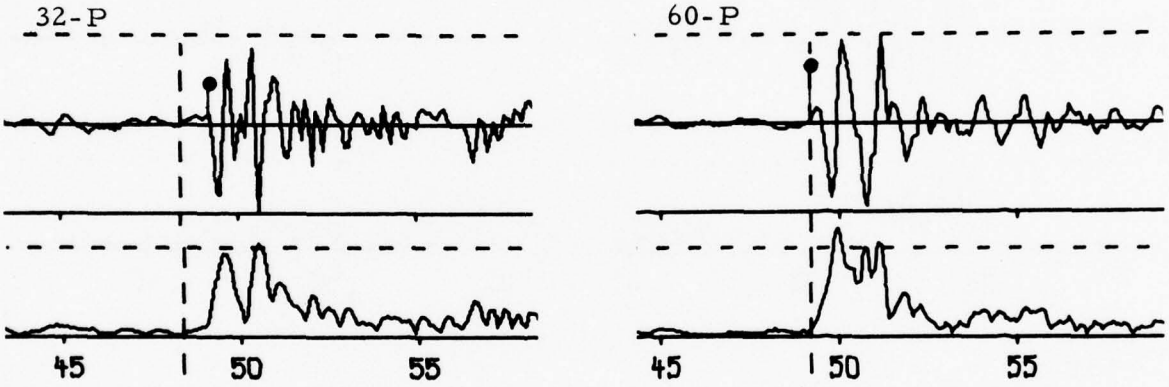

FIGURE IV-1

AUTOMATIC (¦) VERSUS ANALYST (📍) SIGNAL TIMING
(PAGE 5 OF 6)

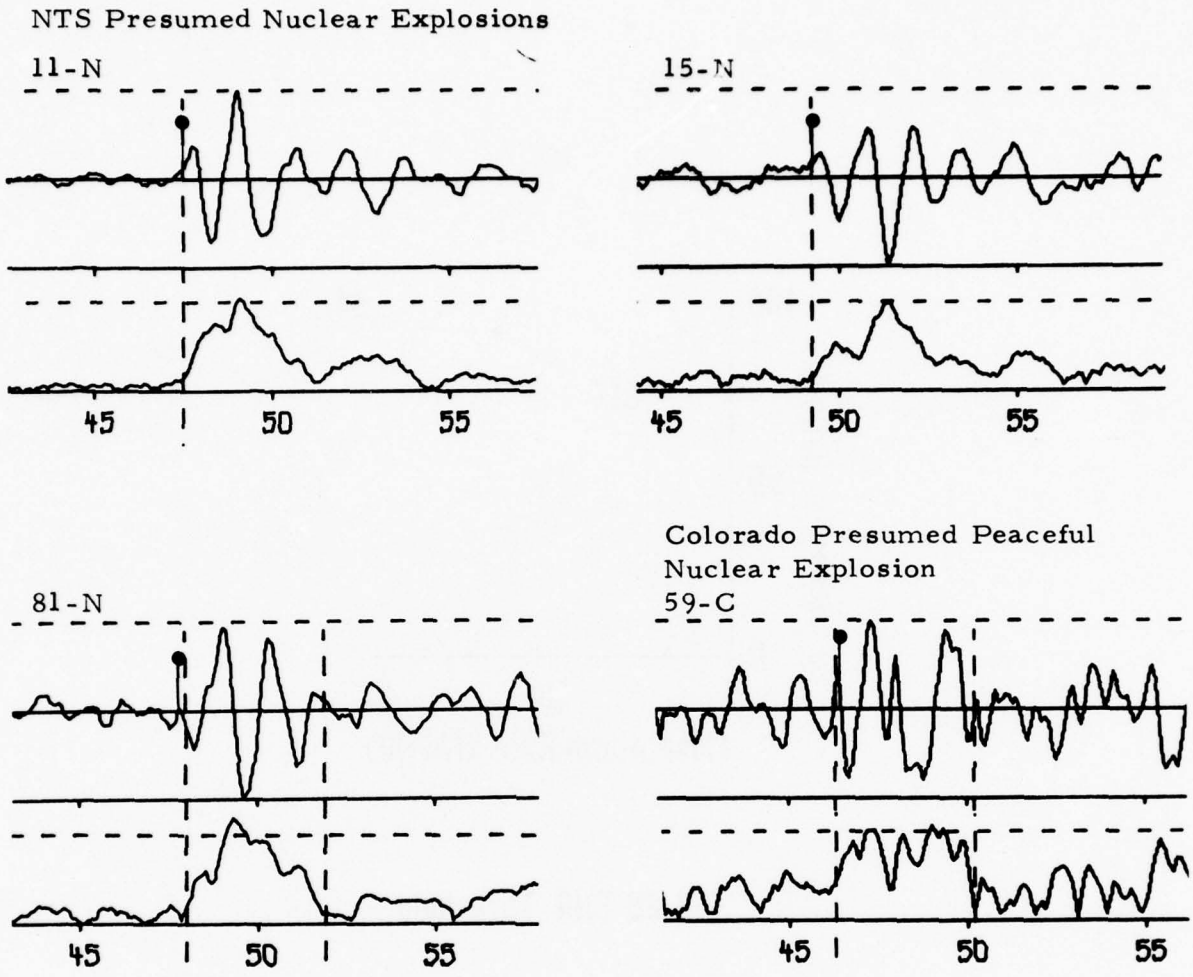

FIGURE IV-1

AUTOMATIC (¦) VERSUS ANALYST (📍) SIGNAL TIMING
(PAGE 6 OF 6)

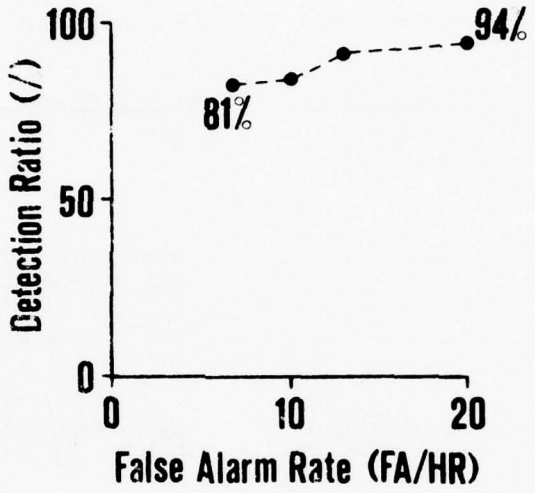

FIGURE IV-2

SP SIGNAL DETECTION CHARACTERISTICS

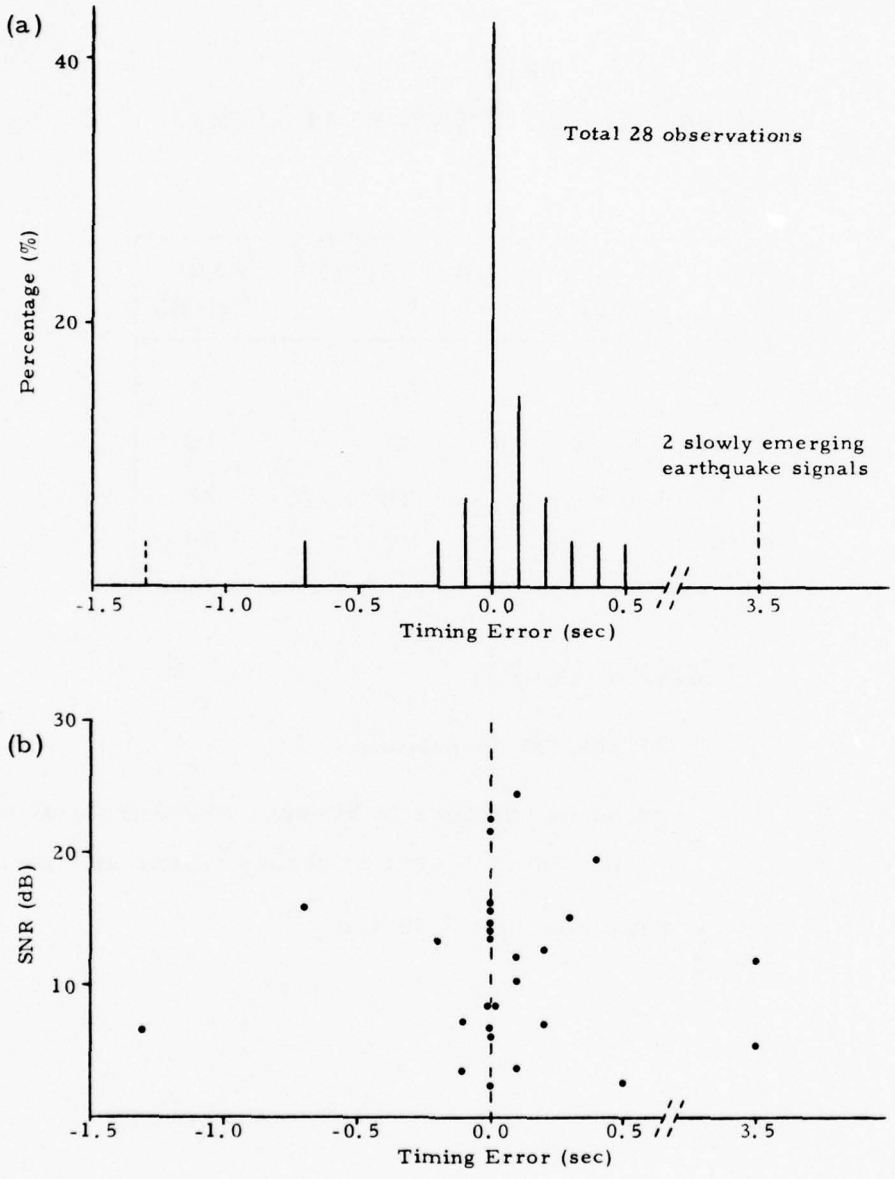

FIGURE IV-3

TIMING ERROR RELATIVE TO ANALYST PICKS

TABLE IV-3

SP SIGNAL DETECTION EVALUATION

TH1	TH2 (dB)	DET RATIO (%)	FAR (FA/H)
0.3	3	81	7
0.3	2	84	10
0.1	3	91	13
0.1	2	94	20

Analysis based on:

31 analyst detections;

35 noise samples of 50-sec average duration, including 20-sec average warm-up time.

time constant = 60 sec

automatic timing errors were estimated to be on the order of -1.3 sec for event 44 and +3.5 sec for events 30 and 38 (indicated by the dotted histogram bars in Figure IV-3a). For one other emergent event (event 89) the onset is so vague that no timing error could be estimated. Figure IV-3b gives the timing errors as a function of SNR of the first detected signal envelope peak (signal envelope peak over noise envelope peak).

The false alarm statistics were derived from the noise parts of the 35 available waveforms, with an average noise duration of approximately 30 seconds after warm-up time. The results suggested that a warm-up time of 30 to 60 seconds is required in on-line applications to avoid excessive false alarm rates. In our evaluation the warm-up time sometimes was taken as short as 10 seconds to allow maximum noise duration before the signal arrival; it was assured that this was not detrimental to the false alarm rate. The thresholds were varied as indicated in Table IV-3.

Besides the timing error evaluation with respect to analyst picks, the behavior of the true timing error for primary and early secondary signals was examined for various noise conditions. This was done by burying some strong signals in a number of different noise samples, at different SNR's. The results are given in Table IV-4; some examples are displayed in Figure IV-4.

Although the algorithm provides, at an elementary level, for signal detection in signal coda, this feature was not considered an immediate objective in the present study. This provision requires further refinement before its performance can be evaluated.

2. Discussion

We observe that at threshold settings of 2 to 3 dB SNR and $P(|\tilde{r}_s(t)| > |\tilde{n}|_{max}) = 10\%$ to 30%, the automatic envelope detector duplicated 81% to 94% of the 31 analyst detections from this particular set of data. Considering only analyst detections from waveforms of less than 12 dB SNR the detection ratios range from 69% to 81% for 16 signals. The false alarm rate

TABLE IV-4

MULTIPLE-SIGNAL ARRIVAL TIMES UNDER NOISE AS INDICATED BY INSTANTANEOUS FREQUENCY EXTREMA

Event	87-Q			58-E			60-P			11-N		
*)	(0)	(1)	(2)	(0)	(1)	(2)	(0)	(1)	(2)	(0)	(1)	(2)
SNR (dB)	12	7	4	15	7	4	23	4	7	16	5	4
Arrival Times (sec)**)			46.1	49.1	49.1	49.0	49.2				46.7	
			46.4	-	-	49.3	49.5	49.6	49.6	47.5	47.3	47.3
		46.5	46.5	49.5	49.6	-	49.8	-	49.7	-	-	47.7
		-	46.6	49.8	49.9	49.8	50.0	50.0	50.0	-	-	48.0
	46.7	-	46.7	50.1	-	-	50.3	50.3	50.2	-	-	48.1
	-	-	47.1	50.3	50.4	50.3	50.4	50.4	50.5	48.4	48.4	48.3
	-	-	47.2	50.5	50.6	-	50.6	50.6	50.6	-	-	48.5
	47.4	-	47.5	50.6	50.7	-	50.8	50.8	50.8	48.8	48.8	48.8
	47.9	-	47.9	50.8	50.8	50.8	51.0	50.9	51.0	49.2	49.5	49.1

*) (0) = original waveform

(1) = original waveform plus low frequency noise sample

(2) = original waveform plus high frequency noise sample.

**) Initial arrival time determined by envelope detection; secondary arrival times are those of extrema in instantaneous frequency. All times relative to record start time.

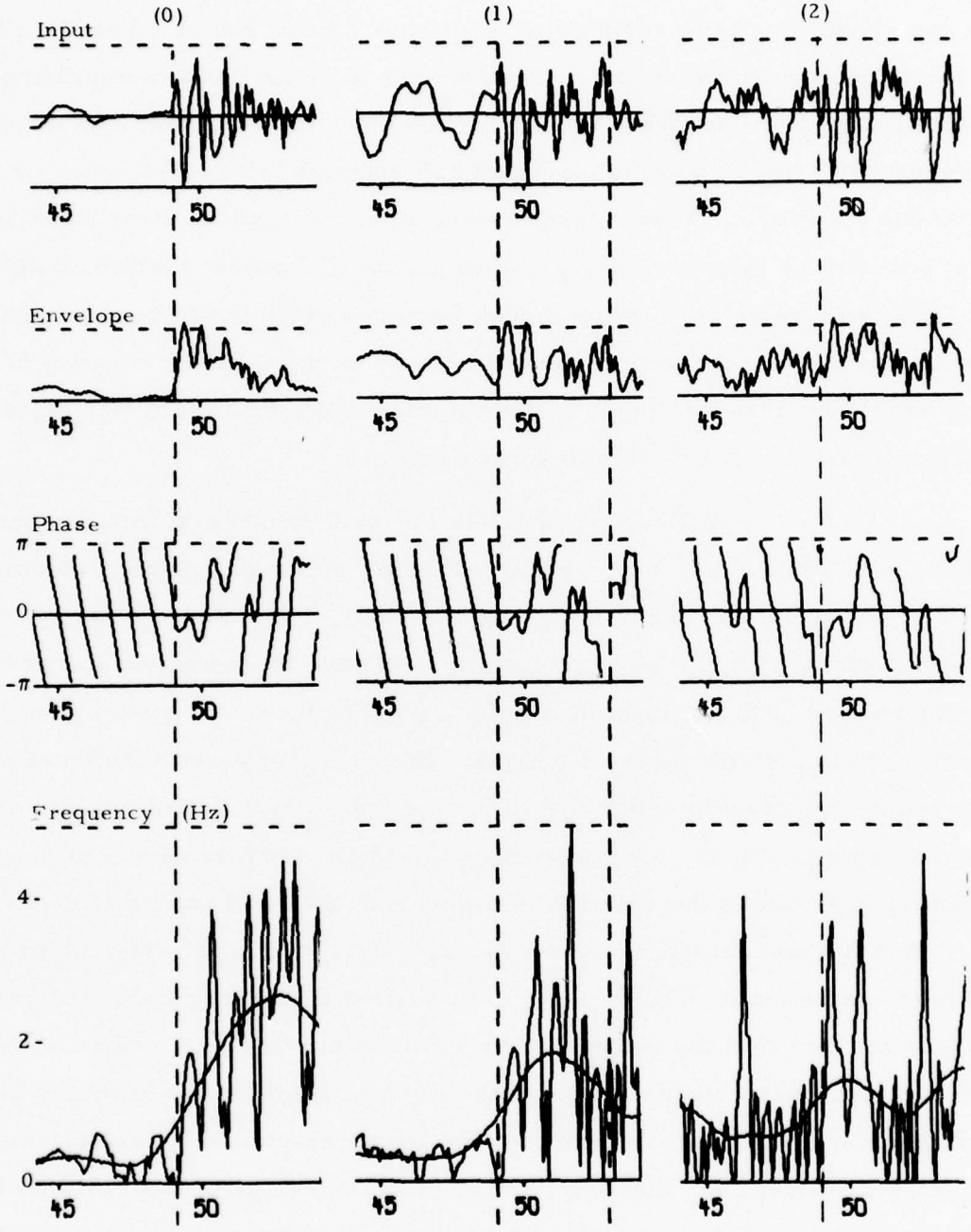

FIGURE IV-4

EFFECTS OF NOISE ON SIGNAL TIMING
(EVENT 58, see TABLE IV-4)

for the above threshold settings ranged from 7 to 20 FA/H. The RMS timing error relative to accurate analyst picks was 0.21 seconds, comprising 84% of this data. Some extreme timing errors were encountered, one about 1.3 seconds early and two on the order of 3.5 seconds late. The latter errors were due to a very gradual signal emergence, causing the first signal envelope peaks to be taken as noise, and to update the 'noise' maximum accordingly. Only when a signal envelope peak becomes sufficiently high it breaks the updating process and a signal detection is declared. Then, because of stepping back from this late peak to find the signal's presumed first quarter period, the signal onset time is determined late.

It is difficult to compare the performance of this detector/timer with that of other ones. A recently developed automatic power detector, to be used in a station processor (Swindell and Snell, 1977) was not designed for accurate signal timing; its timing errors relative to an analyst log are typically on the order of 1.2 seconds. Its detector performance was evaluated on beams of the Korean Seismic Research Station (KSRS). Compared with an analyst log, this power detector detected 76% to 82% of the analyst detections at 7 to 20 false alarms per hour, for power SNR threshold settings of 9.3 to 8.6 dB, respectively. Since the relation between peak SNR and power SNR is not known, and since the two detectors were evaluated using different data, no useful comparison can be made. However, one important difference should be pointed out. This is the fact that the automatic power detector can be operated with a preset, constant false alarm rate. At the present stage in the envelope detector development this is not yet feasible; the alarm rate must be established and adjusted empirically. However, initial noise envelope histograms indicate that the envelope detector probably can also be designed to have a constant false alarm rate; this requires further analysis. Detector performance comparison requires evaluating the detectors with the same data set. Due to incompatibilities in software and data formats such a comparison could not be made during the present study.

In other work, Allen (1976) reports timing local events with 0.05-sec accuracy with one false alarm per hour. These signals, however, have a much higher bandwidth, and are sampled at 200 Hz. Compared to our sampling rate of 10 Hz this means that our RMS timing error of 0.21 sec is very good. Veith (1977) uses Allen's principles also for teleseismic data, but operating characteristics on this work are not available at the present time.

The start times obtained by automatically timing short-period P-waves were evaluated by comparing them to visual analyst picks. The observation that the timing error relative to the analyst pick seems to be independent of the SNR suggests that the problem of consistently accurate timing lies mainly in the variety of signal characteristics, in particular in the initial rise time, and in the rate of emergence (over several envelope peaks) from noise. As our experience grows it may become feasible to characterize signals with respect to these parameters, and to further improve the timing procedure. This additional logic should reduce the probability of extreme timing errors.

During the present study, some thought was given to signal detection and timing with the instantaneous frequency. In dominantly low-frequency noise the frequency in general rises when a signal is present. One then could apply a power or envelope detector to the time series of the instantaneous frequency. However, low-frequency signals, such as those from NTS events,would have a high probability of non-detection. Also, it was found that often the instantaneous frequency rises when no signal is present, in particular where the envelope has a low value. This would result in a relatively high false alarm rate. It would require additional program logic to reduce this false alarm rate by describing the conditions under which a higher frequency reflects the presence of a signal. On the other hand, if such logic could be established, and extended to other observable parameters as well, it could provide a powerful tool in reducing the false alarm rate in general.

The addition of another observable detection parameter in the form of the envelope slope may provide additional contrast between signal and noise waveforms. Other work such as that by *Allen (1976) and Veith (1977)* may also be studied for items which may improve the algorithm's detection and timing characteristics.

Studying the absolute timing error as a function of SNR, we observe that noise may obscure the first signal period or part thereof, or move the first signal envelope peak by interference. This may result in significant timing errors (Table IV-4, Figure IV-4). These phenomena frequently may also escape the analyst's eye. Thus, it is possible that, while the difference between automatic and analyst timing is small, the true timing error in both cases may be significant.

The arrival of secondary signals within the duration of the primary signal causes rapid envelope and phase changes. These arrivals can be timed by locating the rapid changes in the time series of envelope, phase, and frequency, as discussed in Section II. To assess the stability of these changes under various noise conditions, Table IV-4 shows that the relative maxima and minima immediately following the primary signal arrival in the instantaneous frequency time series are in general stable within 0.1 second, down to the primary signal detection level. This means that, if the relative maxima and minima are to be taken as secondary signal arrival indicators, the delays of pP and other early secondary signals can be determined within the duration of any detected SP primary signal. Furthermore, especially in EKZ event signals, we often observed more than one early amplitude and frequency extremum, suggesting the presence of phases other than pP within the first few seconds after the primary signal arrival. This is further discussed in Section V, where this feature is used as event discrimination information.

C. EVALUATION OF THE LP SIGNAL DETECTION AND TIMING ALGORITHM

1. Evaluation

For an initial evaluation of the LP signal detection and timing algorithm, simulated linear chirp signals of 0.015-0.055 Hz, with durations of 300 and 500 seconds, were buried in seven seismic noise samples, at three different time points in each sample, with 4, 2, and 0 dB RMS SNR. This provided 21 independent detection and timing observations for each chirp duration at each of the three SNR's. The RMS SNR was obtained by computing the signal and noise RMS amplitudes, and scaling the signal up to the desired SNR. The noise samples, recorded at stations of the Seismic Research Observatory (SRO), were low-pass filtered at 0.06 Hz with a fourth-order Butterworth filter.

The moving-window quadratic phase regression detector with a priori known dispersion coefficients, described in Section III, was applied to the above waveforms. The regression window length was taken as half the chirp duration, covering only the lower-frequency half of the specified dispersion curve, consistent with the previously stated observation that this part of the dispersion curve is usually well-defined and near-linear. No detection thresholds were set, in order to study the algorithm's dispersion onset timing error as a function of phase s.d. and of phase bias probability. Assuming that, for actual seismic signals, the dispersion onset time is known from the source time and travel time estimates to within $\pm$ 100 seconds, the algorithm-determined dispersion onset was taken as the time of occurrence of either the phase s.d. minimum or the phase bias probability maximum, within a 200-second window about the true chirp onset time.

Figure IV-5 shows the timing error as a function of phase s.d., Figure IV-6 as a function of phase bias probability. In Figure IV-7, the timing errors for the phase s.d. and the phase bias probability are plotted versus SNR. Figure IV-8 shows the phase s.d. and the phase bias probability,

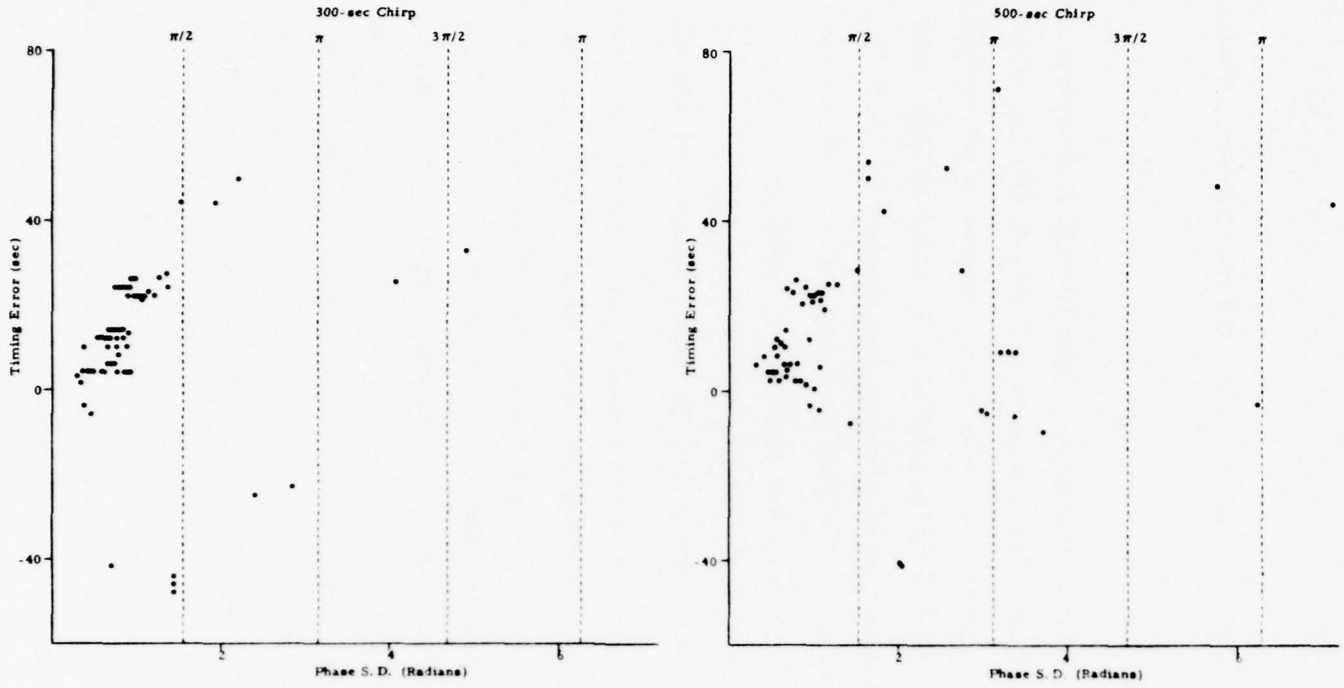

FIGURE IV-5

LP TIMING ERROR VERSUS PHASE S.D.

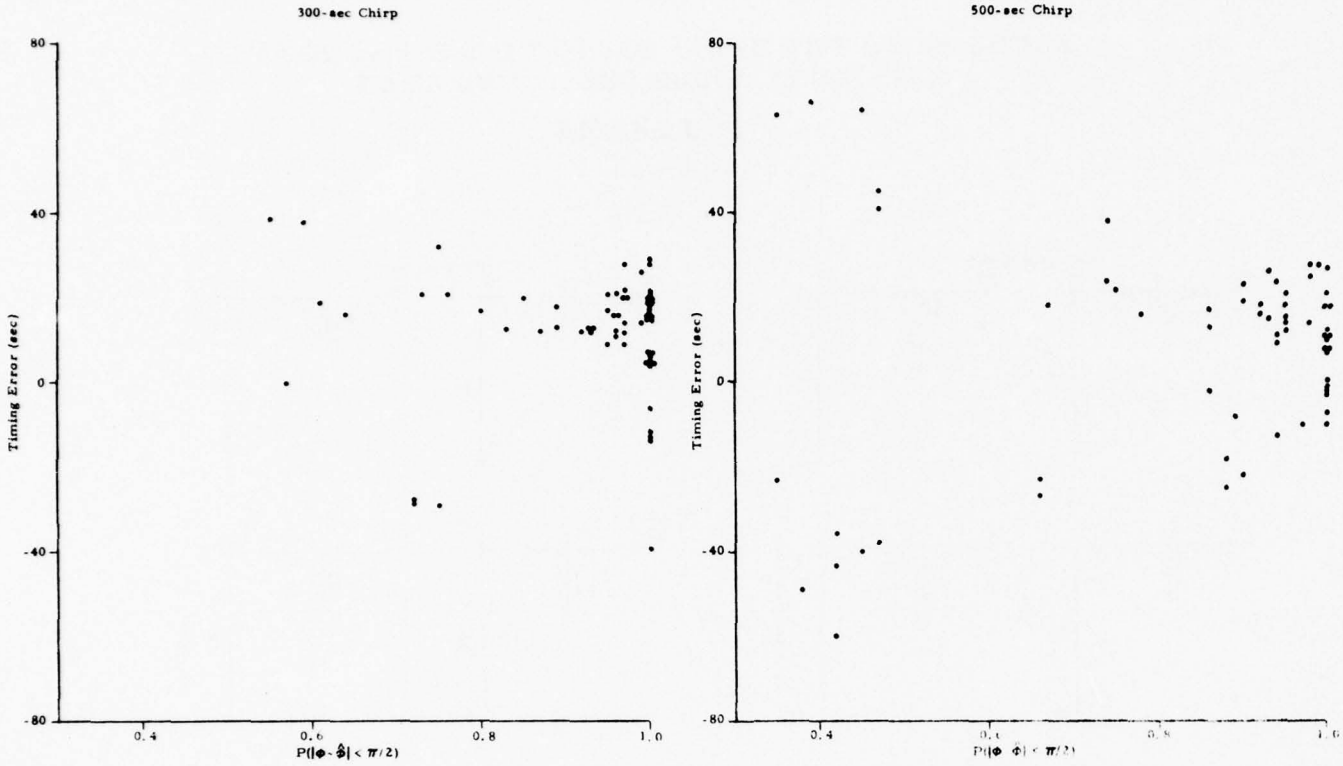

FIGURE IV-6

LP TIMING ERROR VERSUS PHASE BIAS PROBABILITY

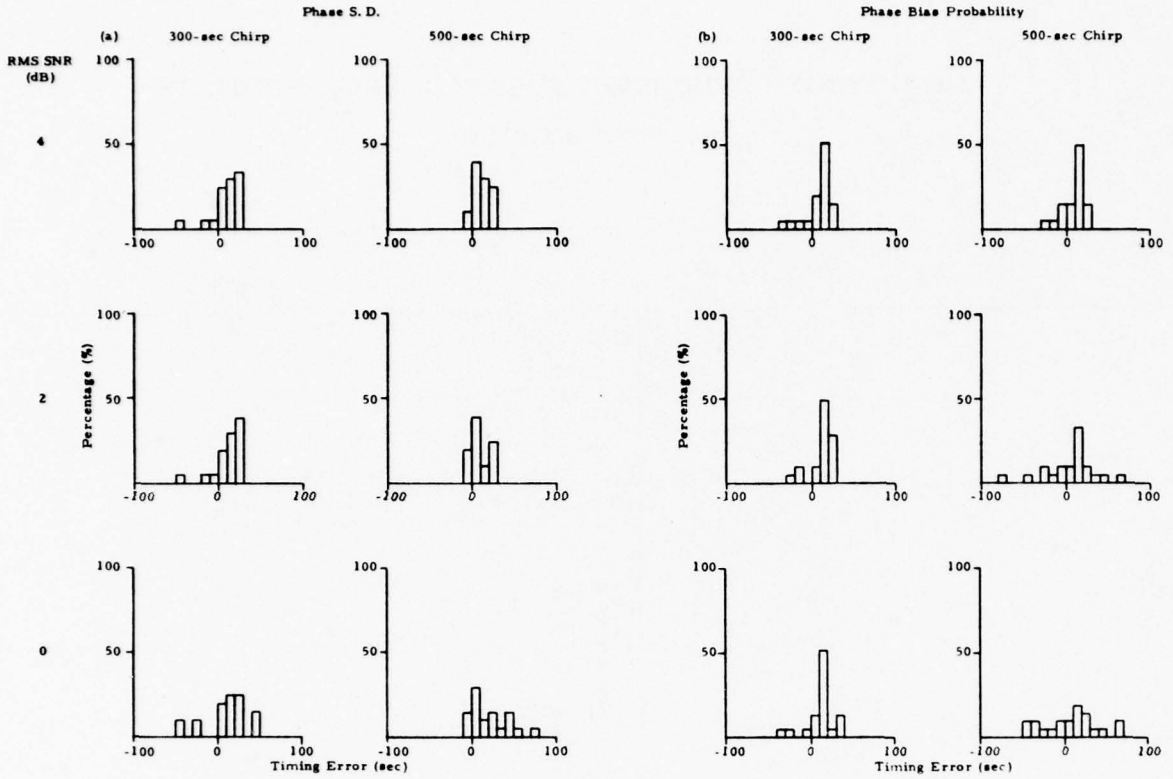

FIGURE IV-7

LP SIGNAL TIMING ERROR VERSUS SNR
(a) FOR PHASE S. D. ; (b) FOR PHASE BIAS PROBABILITY

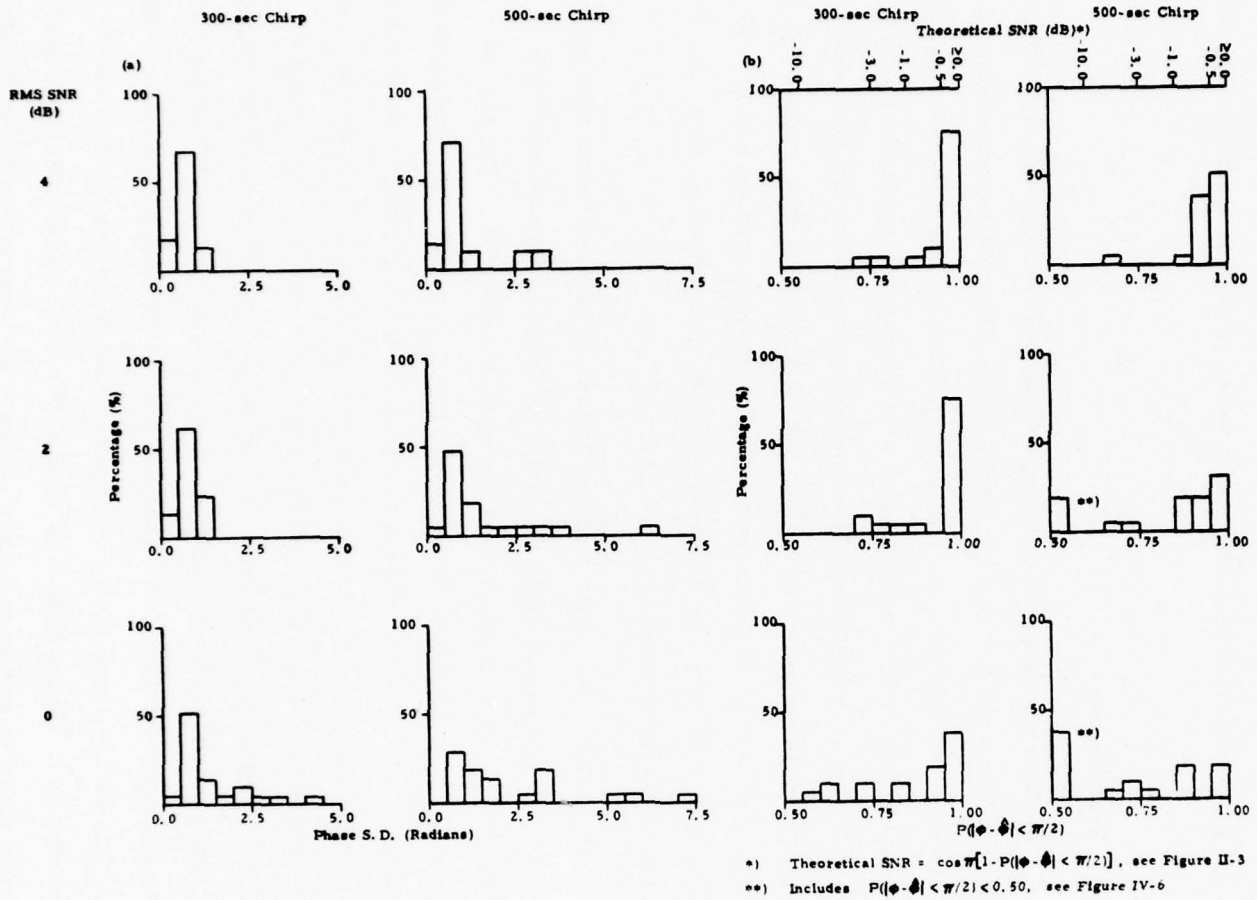

FIGURE IV-8

LP PHASE S. D. (a) AND PHASE BIAS PROBABILITY (b) VERSUS SNR

respectively, as a function of SNR. Finally, Figure IV-9 presents the detection ratio versus false alarm rate, obtained by setting different phase s.d. and phase bias probability threshold levels while processing noise-only waveforms.

2. Discussion

In time-variant, dispersion-related filtering, for a 1000-second, 0.015-0.055 Hz linear chirp signal, timing of the dispersion onset should be accurate to within $\pm$ 50 seconds, to avoid significant amplitude measurement errors ($\Delta \log A > 0.05$) in determining the surface wave magnitude (Unger, 1976b). Steeper sweep rates possibly require a proportionally smaller timing error, depending on the bandwidth used. For instance, a 500-second, 0.015-0.055 Hz chirp then would require less than 25 seconds timing error. In the analysis below, we will focus on the 500-second chirp experiments; the 300-second results are rather similar.

For the 500-second chirp, Figure IV-7a indicates that timing with the phase s.d. minimum at 4, 2, and 0 dB SNR, respectively, 100%, 100%, and 70% of the 21 observations satisfy this criterion. Timing with the phase bias probability maximum generated larger errors. According to measurements in the above-mentioned time-variant filtering study, the maximum timing error of 71 seconds in the present data would not distort the M_s measurement by more than 0.1. Figures IV-5 and IV-6 furthermore suggest that the 25-second timing error limit can be met by setting thresholds of approximately 1.4 radians (80°) upper bound for the phase s.d., and 80% lower bound for the phase bias probability. This would reduce the detection ratio from 100% to 75%, but at the same time also reduce the false alarm rate to 4 false alarms per hour (Figure IV-9). Since in LP signal processing usually the signal onset time is known a priori within $\pm$ 100 seconds, the false alarm rate, computed without regard to this signal arrival time window, probably is of minor concern.

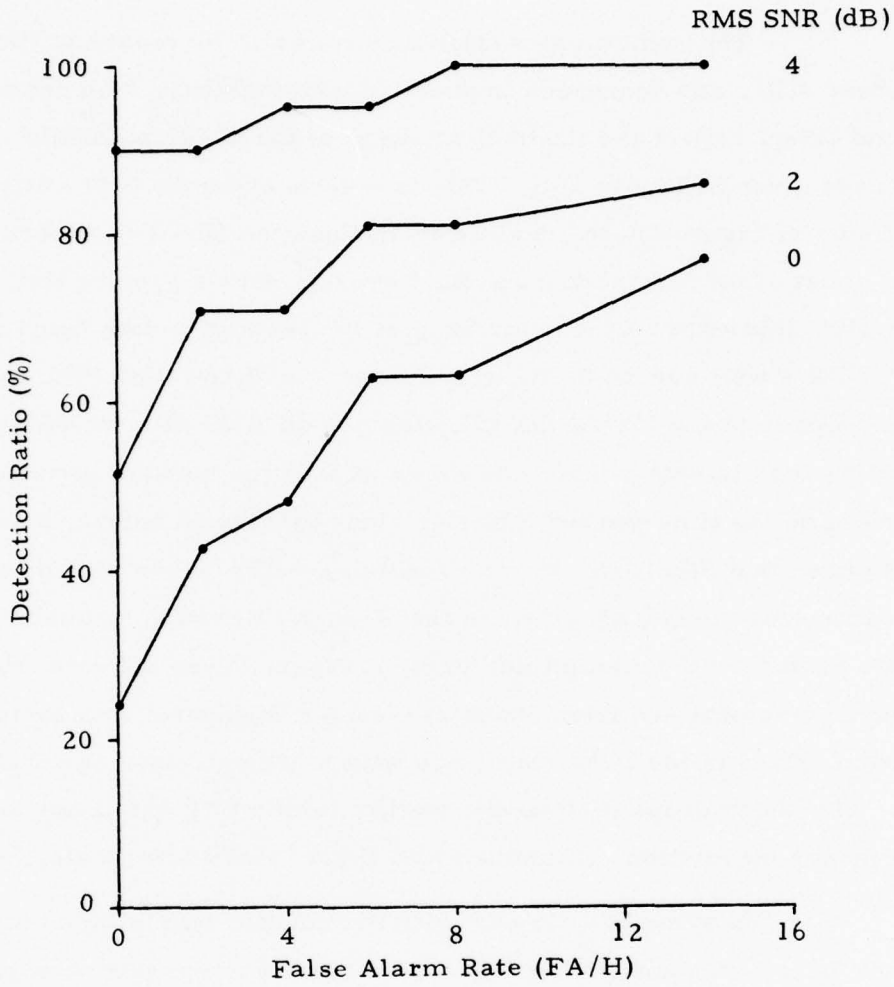

FIGURE IV-9

DETECTION VERSUS FALSE ALARM CHARACTERISTICS OF 500-SEC CHIRP SIGNAL IN $\frac{1}{2}$ HOUR SNZ NOISE SAMPLE* (PHASE BIAS PROBABILITY DETECTION)

*Noise samples at MAI and ANM yielded considerably more favorable characteristics (e.g., 100% detection with 0 FA/H for $\frac{1}{2}$ hour ANM noise sample)

The sometimes sudden and dramatic increases in timing error and phase s.d., and decreases in phase bias probability, with decreasing SNR, to some extent reflect the theoretical shape of the phase probability distribution curve given in Figure II-3. This is evidenced by the SNR scale on the upper side of Figure IV-8b, derived from Equation (II-14). According to this scale, most of the observations reflect average SNR's greater than -1 dB, and those with $P(|\phi - \hat{\phi}| < \pi/2) = 1$ for several consecutive points (such as Figure III-3), SNR's well beyond 0 dB, in accordance with the RMS SNR specified. The sharp drops in phase bias probability for 0-4 dB RMS SNR waveforms may be caused by certain unfavorable interference patterns between signal and noise. According to the time-variant filtering study mentioned before, Wiener filtering requires that SNR's are known to within $\pm$ 4 dB; larger SNR misestimates may cause more than 6 dB error in the Wiener filter gain, translating directly into a 6 dB filter output amplitude error. Figure IV-8b indicates that the SNR measurements obtained from phase regression in general may satisfy this criterion. This needs to be confirmed with more extensive calibrations, however. The sharp drops in detection quality in this SNR range are known also in frequency modulation communications theory (Schwartz et al., 1966).

In summary, in our initial evaluation with simulated chirp signals the LP signal detection and timing method by moving-window phase regression seems to function quite satisfactorily for waveforms above 0 dB SNR. This holds especially true when the algorithm is used to time the onset of a priori known signal dispersions for time-variant, dispersion-related (Wiener) filtering applications. The algorithm furthermore seems to provide SNR information useful in Wiener filtering applications. The method has yet to be tested with real seismic event signals. It is expected that for well-defined dispersion curves, such as those of Sinkiang-ALPA signals (Unger, 1976b) the method will perform as above; problems are to be expected in purely oceanic paths and with overlapping multiple signals.

SECTION V

PRELIMINARY, AUTOMATIC, MULTIVARIATE DISCRIMINATION

A. INTRODUCTION

Since the delay of the pP wave relative to the first P wave is a measure of source depth, its detection and timing can be instrumental in the discrimination between earthquakes and nuclear explosions. Cepstrum analysis of Russian presumed explosions exposed pP delay times of 0.4 to 0.9 seconds (Lane and Sun, 1975; Sun, 1975). Timing early secondary arrivals in eastern Kazakh (EKZ) event signals by detecting rapid changes in the time series of instantaneous amplitude, phase, and frequency yielded delays of supposed pP signals of 0.7 to 0.8 seconds (Unger, 1976a). From this data, as well as in the course of the present study, it was observed in the amplitude, phase, and frequency time series that the first few seconds of EKZ event signals seemed to contain more signal arrivals than just the P and pP waves. The rapid changes in the instantaneous phase, due to multiple signal arrivals, increase the phase error or s.d. in a moving-window phase regression process such as described in Section II and in Appendix A. Thus, this phase s.d., averaged over the regression-window starting points within the first few seconds after the automatically determined P-wave onset, is a potential discrimination parameter.

Furthermore, since an earthquake usually has a finite dimension source and a nuclear explosion more closely resembles a point source, one expects the latter to generate higher frequencies. This has been shown in previous studies for short-period P-waves from Russian presumed explosions as compared to those from Eurasian earthquakes. For instance, Anglin (1971) finds good separation using the third moment of frequency and a measure

of complexity as components in two-variate discrimination. Bache et al. (1976), used a bank of narrowband filters to show the higher frequency content of Russian presumed explosions relative to Eurasian shallow earthquakes. It should be possible to obtain similar results with measurements of the instantaneous frequency.

As the time-variant phase s.d. and the time-variant mean frequency are automatically generated in the moving-window phase regression process developed during this study, the discrimination potential of these two parameters could be readily examined. The evaluation of this potential is described below.

B. AUTOMATIC, MULTIVARIATE DISCRIMINATION EVALUATION

The potential discrimination power of the instantaneous amplitude, phase, and frequency is illustrated in Figure V-1 displaying, respectively, the 0.1-second digitized seismogram. the instantaneous amplitude (envelope), the instantaneous phase, the instantaneous frequency, and the phase s.d., for a Eurasian earthquake, an EKZ presumed nuclear explosion, and a NTS presumed nuclear explosion. The phase s.d. values are plotted at their corresponding window start times in the moving-window phase regression; the window length is 4 seconds. The slowly varying curve in the instantaneous frequency traces is the time-variant mean frequency, computed as the closed-form derivative of the time-variant mean phase regression polynomial, evaluated at the moving-window center (Appendix A).

We notice that the instantaneous frequency values, and the amount of fluctuation in amplitude, phase, and frequency are highest in the EKZ event and lowest in the NTS event. In the earthquake trace an early secondary signal seems to arrive at 0.9 seconds after the primary signal onset, as indicated by the spike in the instantaneous frequency; the next secondary signal does not seem to occur until 3.2 seconds after the primary signal arrival.

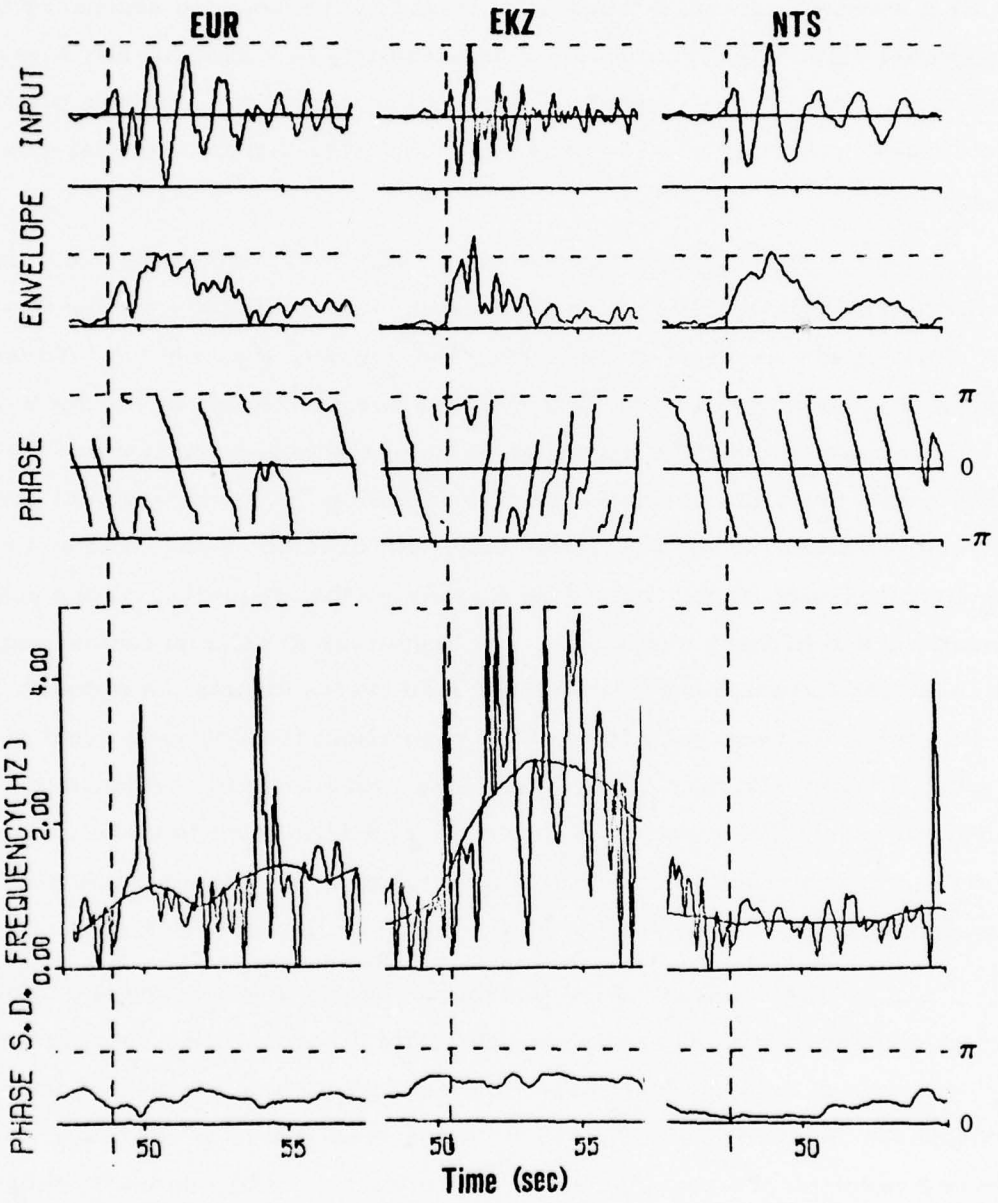

FIGURE V-1

DISCRIMINATION POTENTIAL

The EKZ event signal traces suggest at least four pronounced secondary signal arrivals within the first two seconds, resulting in a significantly higher phase s.d.. In contrast, secondary signals are hardly noticeable in the NTS event traces, resulting in a low phase s.d.; the NTS signal is almost monochromatic.

For the detectable events of Table IV-1, the phase s.d., obtained from moving-window phase regression, was averaged over the window start times in the first two seconds after the primary signal onset. These average phase s.d. values are plotted on the horizontal axis in Figure V-2; the vertical axis depicts the maximum value of the time-variant mean frequency within the 4-second signal window following the primary signal onset. The results show a strong separation between Eurasian earthquakes and presumed nuclear explosions, indicating that either the frequency, or the phase fluctuation, and in many cases both, are higher for Russian presumed explosions than for Eurasian earthquakes; the NTS events display the opposite. One Russian PNE event falls in the EKZ population; the Colorado event and the other Russian PNE are on the borderline with Eurasian earthquakes. Two analyst-detected EKZ events with less than 0 dB SNR seem to classify satisfactorily. These results confirm the spectral multivariate discrimination analysis performed independently by Sax (1976) on the same data set.

The potential of the instantaneous phase and frequency to perform as components in automatic, multivariate discrimination should be further evaluated on a larger data base which should include northern America earthquakes. In particular, the above components should be augmented by including envelope and envelope slope information, and by combining these parameters with those demonstrated by Sax (1976), and other possible discrimination parameters.

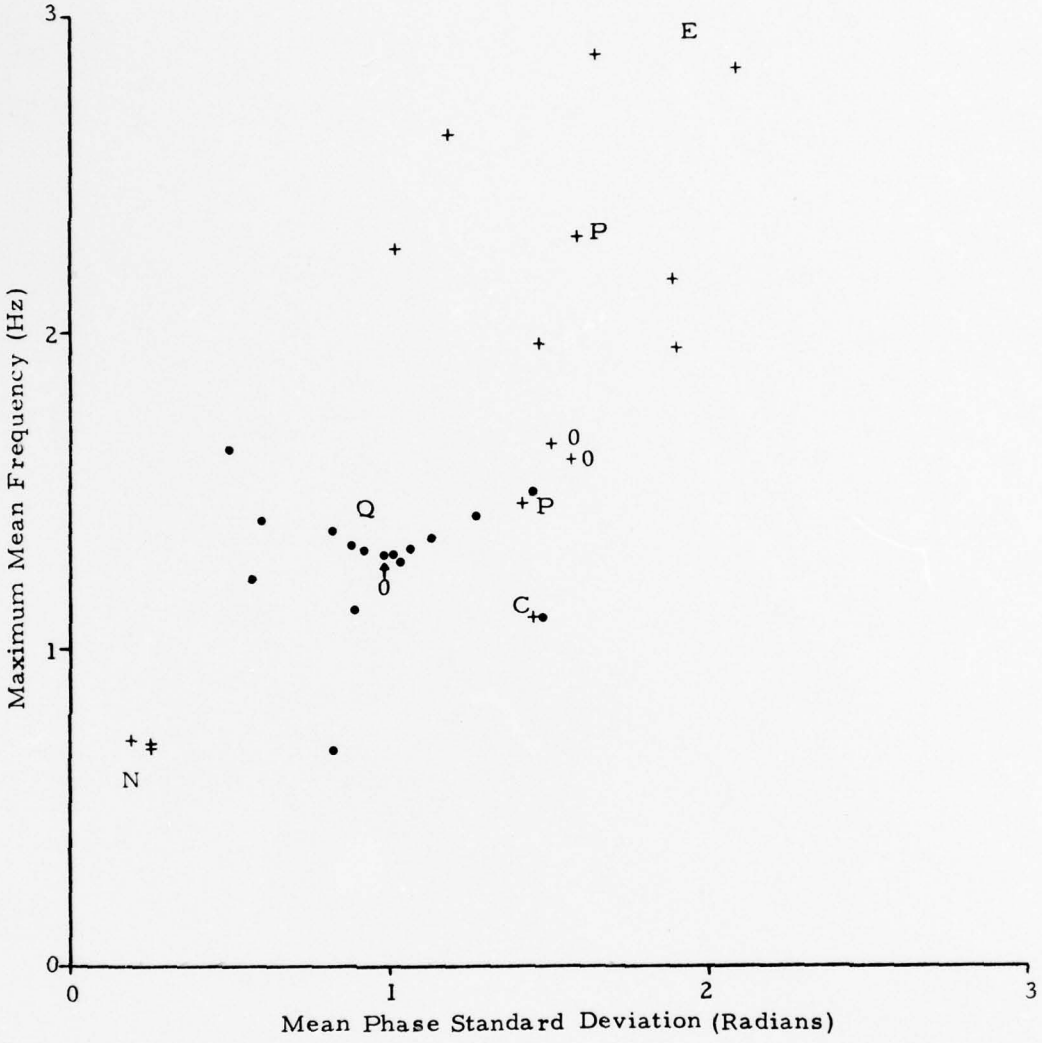

• Q = Eurasian shallow earthquakes

+ E = Eastern Kazakh presumed nuclear explosions

+ P = Russian presumed peaceful nuclear explosions

+ C = Colorado peaceful nuclear explosion

+ N = Nevada Test Site nuclear explosions

•,+ 0 = Event with ≤ 0 dB SNR

FIGURE V-2

NORSAR SINGLE-SITE SP SIGNAL CLASSIFICATION

SECTION VI
SUMMARY

An algorithm for the automatic detection and timing of seismic signals, using the instantaneous amplitude, phase and frequency has been developed, and was evaluated on a limited data base. The instantaneous amplitude, phase, and frequency were furthermore shown to perform as potential components in an automatic, multivariate discriminant. The study led to the following conclusions.

- In theory, statistical phase detection is 6 dB more sensitive than statistical amplitude detection.
- In short-period waveforms, the early arrival of secondary signals renders the phase data unfit for statistical signal detection and timing. Therefore, short-period primary signal detection is performed as peak envelope (instantaneous amplitude) detection, with a frequency-dependent stepback procedure for timing the signal onset.
- For a particular NORSAR data set (which is not necessarily typical) the short-period detection characteristics were: 81% to 94% automatic-detection-over-analyst-detection ratio with 7 to 20 false alarms per hour, at 2 to 3 dB peak-signal-to-peak-noise ratio detection thresholds.
- The short-period RMS timing error for this data set, relative to 25 supposedly accurate analyst picks, is 0.21 seconds, with extremes of 0.7 seconds early and 0.5 seconds late. This error seems to be independent of the signal-to-noise ratio.

However, noise may obscure the actual signal onset for the automatic detector as well as for the analyst, causing significant timing errors for both. In three cases, where analyst picks could not be established better than within one second, the automatic timer may have made errors of up to 3.5 seconds, mainly due to emergent signals.

- The main problem of accurate short-period signal onset timing seems to lie in the variety of initial signal characteristics, such as the rise time and the rate of emergence (over several envelope peaks) from noise. The feasibility of classifying these characteristics should be studied.

- Timing the onset of early secondary signals within the primary signal duration, from sharp maxima and minima in the instantaneous frequency, is stable down to the detection level of primary signals. This allows pP delay time analysis for all detectable primary signals.

- A two-component, multivariate short-period discriminant, using the time-variant mean frequency and the mean-square phase error, both computed through moving-window quadratic regression on the instantaneous phase time series in the signal window, shows a potential separation between Russian presumed nuclear explosions, Eurasian earthquakes, and NTS presumed explosions. In particular, the Russian presumed nuclear explosions, including a peaceful nuclear explosion, display either a higher frequency, or a stronger phase fluctuation, or both, relative to the Eurasian earthquakes; the NTS events show opposite characteristics with near-monochromatic, low frequency signals. Two Russian presumed explosions with waveforms of less than 0 dB signal-to-noise ratio classified

correctly; one Russian presumed peaceful nuclear explosion and a Colorado peaceful nuclear explosion classified close to the earthquake population. The above classification results confirm those obtained independently by Sax (1976).

- The above preliminary characteristics need to be confirmed and augmented by evaluation on a larger data base which should include northern American earthquakes and seismograms recorded at stations other than NORSAR.

- The detection and timing characteristics of the short-period algorithm may be further improved by including the envelope slope as an additional detection and discrimination parameter. Analysis of noise envelope histograms may enable the design of a constant false alarm rate detector.

- Further reduction of the false alarm rate requires adequate definition of false alarms, and the availability of long periods of continuous, analyst-logged data.

- Long-period signals in general lend themselves well for statistical phase detection and timing by means of moving-window quadratic regression on the instantaneous phase, with a priori known dispersion coefficients. This method also produces estimates of the waveform's signal-to-noise ratio, an important parameter in Wiener filtering.

- Timing of the dispersion onset in long-period signals, as simulated with linear chirp signals of various sweep rates and durations, was accurate to within 30 seconds for 100% of the 21 observations at 4 dB and at 2 dB, and for 70% at 0 dB RMS-signal-to-RMS-noise ratio. This is quite adequate for time-variant, dispersion-related filtering applications (Unger, 1976b).

The long-period phase detection and timing algorithm should be further tested on waveforms of real seismic events.

SECTION VII
REFERENCES

Allen, R. V., 1976; Automatic Earthquake Recognition for a Single Trace, Abstract, EOS, 57, 960.

Anglin, F. M., 1971; Discrimination of Earthquakes and Explosions Using Short-Period Seismic Array Data, Nature, 233, 51-52.

Bache, T. C., J. T. Cherry, D. G. Lambert, J. F. Masso, and J. M. Savino, 1976; A Deterministic Methodology for Discriminating Between Earthquakes and Underground Nuclear Explosions, Systems, Science and Software Final Technical Report Number SSS-R-76-2925.

Čiček, V., 1970; Discrete Hilbert Transform, IEEE Transactions on Audio and Electroacoustics, AU-18, 340-343.

Farnbach, J. S., 1975; The Complex Envelope in Seismic Signal Analysis, Bull. Seismol. Soc. Am., 65, 951-962.

Johnson, N. L., and F. C. Leone, 1964; Statistics and Experimental Design in Engineering and the Physical Sciences, Volume I, Wiley & Sons, Inc., New York.

Lane, S. S., and D. Sun, 1975; Counterevasion Studies, Semi-Annual Technical Report No. 4-Part B, Texas Instruments Report No. ALEX(02)-TR-75-01-PART B, AFOSR Contract Number F44620-73-C-0055, Texas Instruments Incorporated, Dallas, TX.

National Bureau of Standards, 1967; Handbook of Mathematical Functions, p. 16, U. S. Government Printing Office, Washington, D. C.

Papoulis, A., 1965; Probability, Random Variables, and Stochastic Processes, McGraw Hill, Inc., New York.

Sax, R. L., and staff, 1974; Seismic Network Systems Study, Special Report No. 17, Extended Array Evaluation Program, Texas Instruments Report No. ALEX(01)-STR-74-01, AFTAC Contract Number F33657-72-C-0725, Texas Instruments Incorporated, Dallas, TX.

Sax, R. L., 1976; Design, Simulated Operation, and Evaluation of a Short-Period Seismic Discrimination Processor in the Context of a World-Wide Seismic Surveillance System, Technical Report No. 9, Texas Instruments Report No. ALEX(01)-TR-76-09, Texas Instruments Incorporated, Dallas, TX.

Schwartz, M., W. R. Bennett, and S. Stein, 1966; Communication Systems and Techniques, McGraw Hill, Inc., New York.

Shen, W. W., 1974; Comparison of Coherent and Incoherent Beamforming Envelope Detectors for NORSAR Regional Seismic Events, Technical Report No. 6, Texas Instruments Report No. ALEX(01)-TR-74-06, AFTAC Contract Number F08606-74-C-0033, Texas Instruments Incorporated, Dallas, TX.

Steinberg, J. C., and T. G. Birdsall, 1966; Underwater Sound Propagation in the Straits of Florida, Jour. Ac. Soc. Am., 39, 301-315.

Sun, D., 1975; Counterevasion Studies, Semi-Annual Technical Report No. 5-Part B, Texas Instruments Report No. ALEX(02)-TR-75-01-PART B, AFOSR Contract Number F44620-73-C-0025, Texas Instruments Incorporated, Dallas, TX.

Swindell, W. H., and N. S. Snell, 1977; Station Processor Automatic Detection System, Phase I: Final Report, Station Processor Software Development, Texas Instruments Report No. ALEX(01)-FR-77-01, AFTAC

Contract Number F08606-76-C-0025, Texas Instruments Incorporated, Dallas, TX.

Unger, R., and R. Veenkant, 1967a; Underwater Sound Propagation in the Straits of Florida: The MIMI Experiment of 3 and 4 February 1965, Technical Report No. 183, Cooley Electronics Laboratory, The University of Michigan, Ann Arbor, MI.

Unger, R., and R. Veenkant, 1967b; Underwater Sound Propagation in the Straits of Florida: The MIMI Continuous and Sampled Receptions of 11, 12, and 13 August 1966, Technical Report No. 186, Cooley Electronics Laboratory, The University of Michigan, Ann Arbor, MI.

Unger, R., 1976a; Seismic Event Discrimination Using the Instantaneous Envelope, Phase and Frequency, Abstract, EOS, 57, 286.

Unger, R., 1976b; A Time-Variant Wiener Filter for Dispersed Waveforms, Technical Report No. 8, Texas Instruments Report No. ALEX(01)-TR-76-08, AFTAC Contract Number F08606-76-C-0011, Texas Instruments Incorporated, Dallas, TX.

Unger, R., 1976c; The Instantaneous Phase of Long-Period Waveforms, Abstract, EOS, 57, 759.

Veith, K. F., 1977; A Digital Event Detector, Abstract, EOS, 58, 1190.

APPENDIX A

MOVING-WINDOW QUADRATIC PHASE REGRESSION

Below we discuss details of the phase regression analysis algorithm used in the automatic detection, timing and discrimination of seismic signals. A quadratic phase regression model was chosen since this reflects linearly dispersed signals in long-period waveforms, and also seems to satisfy most short-period signal phase patterns before the arrival of secondary signals. The algorithm performs regression on a window of given length in the 'continuous' instantaneous phase time series. The window then is moved up one sample and the process is repeated, until the window reaches the end of the waveform.

Within each window of user-defined length, the instantaneous phase function is approximated with a quadratic polynomial:

$$\hat{\phi}(t, \tau) = a_0(t) + a_1(t)\tau + a_2(t)\tau^2 \qquad \text{(A-1)}$$

where

- t is the window start time,
- τ is the relative time within the window,
- $\hat{\phi}(t,\tau)$ is the estimated instantaneous phase function for the window starting at time t,
- $a_0(t)$ is the initial phase for this window,
- $a_1(t)$ is the window's first order coefficient, reflecting the lowest frequency of the dispersion curve,

$a_2(t)$ is the window's second order coefficient reflecting the dispersion curve's sweep rate (frequency increment/ time increment).

In the phase regression process, this polynomial is fit with minimum mean-square error to the time series of the 'continuous' instantaneous phase, $\phi(t,\tau)$, within the window. This yields, for each window start time, the coefficients $a_0(t)$, $a_1(t)$ and $a_2(t)$ (e.g., Johnson and Leone, 1964):

$$a_1(t) = \left[L\left(\sum_i \phi_i i \sum_i i^4 - \sum_i \phi_i i^2 \sum_i i^3\right) - \sum_i \phi_i \left(\sum_i i \sum_i i^4 - \sum_i i^2 \sum_i i^3\right) + \sum_i i^2 \left(\sum_i \phi_i i^2 \sum_i i - \sum_i \phi_i i \sum_i i^2\right)\right] / \Delta \qquad (A-2)$$

$$a_2(t) = \left[L\left(\sum_i \phi_i i^2 - a_1(t) \sum_i i^3\right) - \left(\sum_i \phi_i - a_1(t) \sum_i i\right) \sum_i i^2 \right] / \left[L \sum_i i^4 - \left(\sum_i i^2\right)^2 \right] \qquad (A-3)$$

$$a_0(t) = \left[\sum_i \phi_i - a_2(t) \sum_i i^2 - a_1(t) \sum_i i \right] / L \qquad (A-4)$$

where

$$\Delta = L\left(\sum_i i^2 \sum_i i^4 - \sum_i i^3 \sum_i i^3\right) - \sum_i i \left(\sum_i i \sum_i i^4 - \sum_i i^2 \sum_i i^3\right) + \sum_i i^2 \left(\sum_i i \sum_i i^3 - \sum_i i^2 \sum_i i^2\right) \qquad (A-5)$$

and L is the number of data points within a window;

i is the data point index within a window; i=1, 2, . . . , L;

ϕ_i is the 'continuous' phase at the i^{th} data point.

The summations $\sum i$, $\sum i^2$, $\sum i^3$, and $\sum i^4$ can be calculated with the Euler-MacLaurin summation formula (National Bureau of Standards, 1964):

$$\sum_{k=1}^{n-1} f_k = \int_o^n f(k)dk - \frac{1}{2}\left[f(o) + f(n)\right] + \frac{1}{12}\left[f'(n) - f'(o)\right]$$

$$- \frac{1}{720}\left[f'''(n) - f'''(o)\right] + \text{------} \qquad \text{(A-6)}$$

For the above summations this results in:

$$\sum_{i=1}^{L} i = \frac{1}{2}(L+1)^2 - \frac{1}{2}(L+1) \qquad \text{(A-7)}$$

$$\sum_{i=1}^{L} i^2 = \frac{1}{3}(L+1)^3 - \frac{1}{2}(L+1)^2 + \frac{1}{6}(L+1) \qquad \text{(A-8)}$$

$$\sum_{i=1}^{L} i^3 = \frac{1}{4}(L+1)^4 - \frac{1}{2}(L+1)^3 + \frac{1}{4}(L+1)^2 - \frac{1}{120} \qquad \text{(A-9)}$$

$$\sum_{i=1}^{L} i^4 = \frac{1}{5}(L+1)^5 - \frac{1}{2}(L+1)^4 + \frac{1}{3}(L+1)^3 - \frac{1}{30}(L+1) \qquad \text{(A-10)}$$

The phase standard deviation for each window is (Johnson and Leone, 1964):

$$\sigma_\phi(t) = \left\{\sum_{i=1}^{L}\left[\phi(t,\tau_i) - \hat{\phi}(t,\tau_i)\right]^2/(L-3)\right\}^{\frac{1}{2}} \qquad \text{(A-11)}$$

We define the time-variant mean phase as the regressed phase evaluated at each window center ($\tau = L/2$):

$$\bar{\phi}(t + L/2) \triangleq \hat{\phi}(t, L/2)$$

$$= a_o(t) + \frac{L}{2} a_1(t) + \frac{L^2}{4} a_2(t) \qquad \text{(A-12)}$$

The time-variant mean frequency is found by differentiating $\hat{\phi}(t, \tau)$ with respect to τ, and evaluating at $\tau = L/2$:

$$\bar{f}(t + \frac{L}{2}) = \left[a_1(t) + L\, a_2(t) \right] / 2\pi \qquad \text{(A-13)}$$

For the detection and timing of long-period signals with a priori known linear dispersion curves, the phase regression process reduces to Equation (A-4) with $a_1(t)$ and $a_2(t)$ known.

APPENDIX B

ENVELOPE AND PHASE DETECTION PROBABILITY FUNCTIONS

The envelope and phase detection probability functions used in Section II follow immediately from the vectordiagram situations in Figure B-1. We assume a uniformly distributed instantaneous noise phase angle, $\phi_n(t)$.

For a given instantaneous SNR between 0 and 2, the probability that the instantaneous waveform amplitude, $|\vec{r}(t)|$, is greater than the instantaneous noise amplitude, $|\vec{n}(t)|$, is the thickened arc in Figure B-1a, divided by 2π. For a given instantaneous SNR between 0 and 1, the probability that the instantaneous phase is less than 90° is the thickened arc in Figure B-1b, divided by 2π. This results in:

$$P(|\vec{r}(t)|>|\vec{n}(t)|) = 1-\pi^{-1}\arccos(|\vec{s}(t)|/2|\vec{n}(t)|), \quad 0<|\vec{s}(t)|/|\vec{n}(t)|\leq 2 \tag{B-1}$$

and

$$P(|\phi(t)| < \pi/2) = 1-\pi^{-1}\arccos(|\vec{s}(t)|/|\vec{n}(t)|), \quad 0\leq|\vec{s}(t)|/|\vec{n}(t)|\leq 1. \tag{B-2}$$

The envelope detection probability function has a discontinuity for $|\vec{s}(t)|/|\vec{n}(t)| = 0$, since, when no signal is present, $|\vec{r}(t)| = |\vec{n}(t)|$ so that

$$P(|\vec{r}(t)|>|\vec{n}(t)|) = 0, \qquad s(t) = 0, \tag{B-3}$$

but for an infinitesimally small signal this probability equals 50%:

$$\lim_{s(t)\to 0} P(|\vec{r}(t)|>|\vec{n}(t)|) = 0.5 \tag{B-4}$$

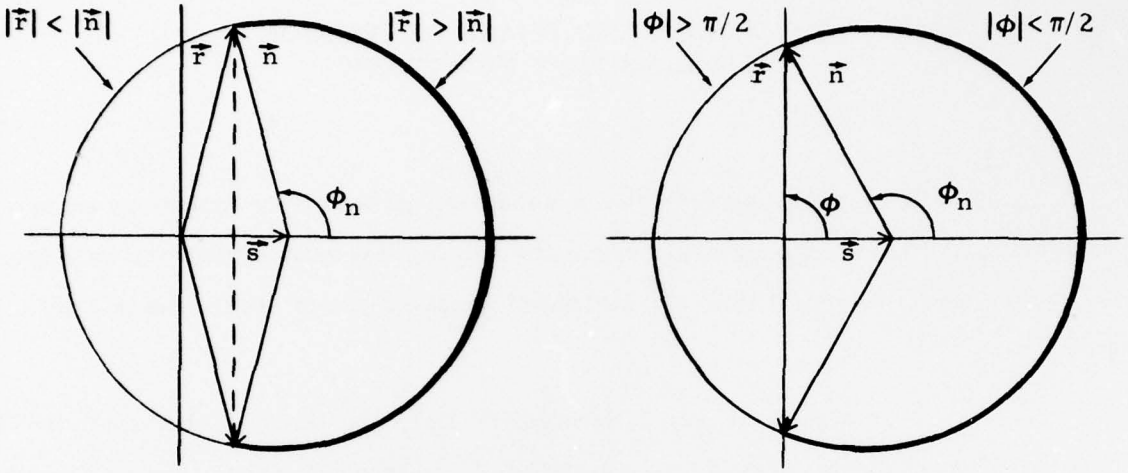

(a) Envelope Detection

(b) Phase Detection

FIGURE B-1

VECTORDIAGRAM GEOMETRY FOR ENVELOPE AND PHASE DETECTION

The phase bias probability is 50% in both cases, since then $\phi(t) = \phi_n(t)$ which was assumed to be uniformly distributed.

For $|\vec{s}(t)| / |\vec{n}(t)| > 2$, always $|\vec{r}(t)| > |\vec{n}(t)|$, so that

$$P(|\vec{r}(t)| > |\vec{n}(t)|) = 1, \qquad |\vec{s}(t)| / |\vec{n}(t)| > 2 \quad . \tag{B-5}$$

For $|\vec{s}(t)| / |\vec{n}(t)| > 1$, always $|\phi(t)| < \pi/2$, so that

$$P(|\phi(t)| < \pi/2) = 1, \qquad |\vec{s}(t)| / |\vec{n}(t)| > 1. \tag{B-6}$$

The above indicates that, in principle, phase detection is 6 dB more sensitive than amplitude detection. The probability functions are sketched in Figure II-3.